IEEE Access
Multidisciplinary | Rapid Review | Open Access Journal

IEEE POWER & ENERGY SOCIETY SECTION

Received 10 October 2023, accepted 20 November 2023, date of publication 21 November 2023,
date of current version 30 November 2023.

Digital Object Identifier 10.1109/ACCESS.2023.3335902

RESEARCH ARTICLE

Fractional-Order Synergetic Control of the Asynchronous Generator-Based Variable-Speed Multi-Rotor Wind Power Systems

HABIB BENBOUHENNI[1], MOHAMED I. MOSAAD[2], (Senior Member, IEEE), ILHAMI COLAK[1], NICU BIZON[3,4,5], (Senior Member, IEEE), HAMZA GASMI[6], MANSOUR ALJOHANI[2], AND EMAD ABDELKARIM[7,8]

[1]Department of Electrical and Electronics Engineering, Faculty of Engineering and Architecture, Nisantasi University, 34481742 Istanbul, Turkey
[2]Yanbu Industrial College (YIC), Alnahdah, Yanbu 46452, Saudi Arabia
[3]Piteşti University Centre, National University of Science and Technology POLITEHNICA Bucharest, 110040 Pitesti, Romania
[4]Institute Doctoral School, Polytechnic University of Bucharest, 060042 Bucharest, Romania
[5]ICSI Energy, National Research and Development Institute for Cryogenic and Isotopic Technologies, 240050 Ramnicu Valcea, Romania
[6]Laboratoire de Contrôle Avancé (LABCAV), Department of Electronics and Telecommunications, University of Guelma, Guelma 24000, Algeria
[7]Department of Electrical Engineering, University of Electric Engineering Aswan, Aswan 81542, Egypt
[8]Department of Electric Engineering, Buraydah Private Colleges, Buraydah, Qassim 51418, Saudi Arabia

Corresponding author: Mohamed I. Mosaad (m_i_mosaad@hotmail.com)

ABSTRACT This work provides regulation of active and reactive power for asynchronous generator-based multi-rotor wind power (MRWP) systems using a synergetic control based on fractional order control theory. The traditional synergetic control theory achieves an undesirable chattering effect, which can damage the system. For this, it is relevant to combine the traditional synergetic control theory with fractional order control to avoid these drawbacks. Two control schemes are proposed, analyzed, and compared: traditional direct power control (DPC) and DPC based on fractional-order synergetic controllers, the latter needs only the information of the sliding surface. Their characteristics are compared in terms of current quality, active and reactive power reference tracking, robustness against generator parameter variations, and power ripple. Simulation results using Matlab software have demonstrated the characteristics and robustness of the suggested DPC based on fractional-order synergetic controllers compared to the DPC because of its efficacy in improving the quality of power/current.

INDEX TERMS Asynchronous generator, direct power control, multi-rotor wind power, fractional order control, synergetic control theory.

NOMENCLATURE

AG	Asynchronous generator.
DFIG	Double-Fed Induction generator.
DPC	Direct power control.
DTC	Direct torque control.
FL	Fuzzy logic.
FOC	Field-oriented control.
FOSC	Fractional-order synergetic control.
IPWM	Intelligent pulse width modulation.
MRWP	Multi-rotor wind power.
MPPT	Maximum power point tracking.
MSVM	Modified space vector modulation.
R_r	Stator resistance.
NSTA	Neural super twisting algorithm.
PI	Proportional-integral.
PWM	Pulse width modulation.
SMC	Sliding mode control.
SSMC	Synergetic-sliding mode control.
SSE	Steady-state error.
STA	Super twisting algorithm.
THD	Total harmonic distortion.
TSC	Terminal synergetic control.

The associate editor coordinating the review of this manuscript and approving it for publication was Sinisa Djurovic.

VC Vector control.
WP Wind power.
R_s Rotor resistance.

I. INTRODUCTION

The traditional direct power control (DPC) of asynchronous generator-based multi-rotor wind power (AG-MRWP) systems has a quick active power (*Ps*) response without inner loop current control and complex orientation transformation [1]. This strategy belongs to the family of linear strategies, as it uses a switching table (ST) to generate control pulses in the inverter. Two classical hysteresis comparators (HCs) are used to regulate the output power. In principle and idea, the DPC has the same characteristics and advantages of the direct torque control (DTC); however, they differ in the references used only. In the DPC, both *Ps* and reactive power (*Qs*) are used as references, while in the DTC, both torque and flux are used as references. As compared to other strategies like backstepping control (BC) and vector control (VC), this control is considered to be the simplest and most straightforward [2]. Although DPC has some disadvantages, such as the total harmonic distortion (THD) of current and *Ps* ripples [3]. These defects are among the problems in the wind turbine system (WTS) and affect its spread and limit its use. Therefore, it is necessary to reduce these shortcomings and try to overcome them to increase the robustness of the WTS. Also, this strategy is greatly affected by the change of system parameters and this is shown by the high rate of ripples and the value of THD of current. The important point in the DPC is the proper selection of the rotor voltage vector. Compared to VC and field-oriented control (FOC), DPC does not use inner loops that increase the complexity of the system and reduce the robustness of the strategy [1], [2]. To command the power, two different level HCs are used, where a 3-level HC is used to control the *Ps* and a 2-level HC is used to control the *Qs* [3]. The widespread use of the DPC is constrained by the usage of these traditional controls, which significantly increase THD at the level of voltage and current. In addition to these controllers, the full *Ps* and *Qs* rating is used, where the power rating is linked to the voltage and current measuring devices. Therefore, high-efficiency measuring devices must be used, which increases the cost of the system as a whole.

Several studies have proven that the use of a HC in the DPC is the cause of fluctuations in the power level and in decreasing the quality of the current [1], [3]. Also, several solutions have been suggested to increase efficiency and overcome the problems of the DPC [4], [5], [6], [7], [8], [9]. Most of these solutions that have been proposed to overcome the defects of DPC are dispensed with ST and two HCs, as they are compensated with other techniques, which may lead to an increase in the complexity and thus the difficulty of implementation, and this is undesirable. Among these suggested solutions, we can mention the nonlinear controls, which are the sliding mode control (SMC) [4] and the BC technique [5]. Nonlinear strategies are characterized by durability, are not affected much by changes in system parameters, and have the ability to improve the dynamic response of systems compared to the linear strategies [4], [5]. However, applying nonlinear controls has drawbacks, including complexity, which is characterized by implementation challenges, particularly in complex systems [6]. Moreover, the use of nonlinear controls increases the cost of industrialization. This is undesirable, which creates several problems at the level of power generation systems. A DPC-BC for *Ps* and *Qs* control of an AG-based wind power (WP) system has been introduced in [7], where a BC was designed to calculate the stator direct and quadrature voltage references. In this strategy, power ripples are to some extent overcome and current quality is increased compared to DPC. However, there remains a negative aspect of the high degree of complexity, which makes it difficult and more expensive to complete. In addition, there are many parameters, which makes it difficult to adjust the dynamic response of the power and this is not desirable. In [8], a nonlinear control was designed to calculate the AG rotor voltage controlled by the DPC. This nonlinear control theory is based on the SMC. In this strategy, ST and two HCs were compensated for by SMC and pulse width modulation (PWM). Although the SMC has shown high characteristics, still the controller becomes complex and error-prone with the parameter differences because it depends on the AG parameters. So the control ring must be fine-tuned. The negativity of the proposed control in [8] is represented in relying on the estimation of powers to calculate the error, which creates problems in case of changing the system parameters. Also, the SMC is related to the mathematical form of the studied system, which makes it difficult to adjust the response and increases the value of ripples in the event of a defect in the system. In addition, the DPC (which was first proposed in [9] for an AG-WP system) has good dynamic performance and lowers *Ps* and *Qs* ripples compared to FOC and VC strategies. Despite the high robustness that characterizes this strategy and the results obtained, there is a negative one represented in relying on power estimation, and this requires the use of highly efficient measurement devices to reduce the error in powers. In addition, there is a chatterbox that creates problems in the system. A DPC was suggested in [10] in which synergetic control (SC) theory was used instead of hysteresis control loops to calculate the rotor voltage, and the ST was replaced by the modified space vector modulation (MSVM). Both the *Ps* and *Qs* are estimated in this proposed DPC, which requires high-quality measuring devices. The advantage of the DPC-SC is simplicity, ease of adjusting results, and inexpensive, which makes it among the reliable solutions. Through the obtained results, it was found that the DPC-SC is highly efficient compared to the DPC, and the simplicity of the algorithm is among its strongest features. Despite these results presented in the various tests carried out, it is noted that in the event of a change in the system parameters, an increase in the ripple ratio is observed as a result of the use of power estimation, and this is undesirable. A robust DPC was designed in [11], where the *Ps* and *Qs* of AG are calculated using a neural

super-twisting algorithm (NSTA) and the rotor inverter is controlled by MSVM. This strategy is completely different from DPC, where the ST is dispensed with and replaced by the MSVM technique. Compared to DPC, this strategy is complex and uses the same power estimation formulas, which may create drawbacks in this control if the system parameters change. Simulation results showed that the DPC-NSTA is more efficient and robust than the DPC in the case of changing the generator parameters. The fractional-order DPC was proposed in [12], in which the behaviour of the strategy was examined in case of changing the generator parameters compared to the DPC. In this strategy, fractional calculus was applied to the proportional-integral (PI) controller for power control, two fractional-order PI controllers were used for this purpose. To control the inverter, PWM was used to generate the necessary signals. The proposed control is fairly simple, and the robustness of the system has been increased compared to using DPC. However, the presence of ripples in the energy level, torque, and current is noticed, as they were not completely eliminated, and this is the result of using the capacity assessment. In [13], a robust continuous-time model predictive DPC (PDPC) for AG-based wind turbines is proposed. The suggested approach uses Taylor series expansion to predict the stator current in the synchronous reference frame over a finite time horizon. In this PDPC, the predicted stator current is directly used to compute the required rotor voltage to reduce the difference between the actual stator currents and their references over the predictive time. However, as the PDPC is sensitive to parameter variations and external disturbances, a disturbance observer is embedded into the control loop to remove the steady-state error (SSE) of the current. The PDPC was experimentally verified for network-connected DFIG compared to the DPC, and the obtained results were very satisfactory with high performance. A fuzzy logic (FL) has been proposed to overcome the disadvantages of DPC as in [14]. In this intelligent DPC, the FL controller is used for adjusting the bandwidth of the PS-HC in the DPC to minimize *Ps* ripples and improve dynamic AG response. This strategy was applied to 2MW AG using Matlab software, and the presented results proved the efficiency and high ability of the proposed strategy in improving the system properties. The negative of using FL is represented in the absence of a rule that defines how the number of rules is determined to control, as the more the number of rules, the slower the system becomes, and this is undesirable. In [15], an adaptive neuro-fuzzy algorithm was used to reduce the power ripples of the AG controlled by DPC. This strategy has been proposed to deal with grid-side perturbation and realize low-voltage ride-through capabilities by controlling the rotor-side converter (RSC) based on the errors between the *Ps* and *Qs* of the stator with their corresponding reference values. In [16], the authors combined DPC and VC strategies to control the AG-WP inverter, and thus the performance of the resulting technique (quality of current and power ripple ratio) became better than the DPC and VC strategies. This strategy has a downside, which is the presence of a kind of complexity, which makes it difficult to implement. Also, it depends on power estimation, and this is undesirable, as ripples are observed in the current, which creates problems at the network level. In [17], a perturbation observer-based DPC was proposed to control the AG using two-stage Kalman filters. This strategy does not need to know the mathematical form of the system (generators) or the presence of eddy current sensors, which increases its durability, especially in the case of changing the system parameters. Simulation results prove the high performance and the ability of this strategy to reduce power ripples in case of system parameters change. A 3-vector-based low-complexity model predictive (LCMP) was designed to improve the DPC [18]. This three-vector DPC-LCMP which is different from the DPC in principle and degree of complexity is designed to control the AG power. Both simulations and experimental results indicate that the designed 3-vector DPC-LCMP can significantly improve steady-state performance and achieve error-free control. In addition, its dynamic performance remains satisfactory compared to the DPC-LCMP based on a single or binary vector.

SC technique, as a simple and easy-to-implement nonlinear strategy, has multiple advantages over other nonlinear strategies, such as ease of application to systems, reduced chattering problems, low chattering, and high robustness [19]. Due to the simplicity of implementation, SC can be proposed to control complex systems, such as 7-phase motors. So simple nonlinear methods become attractive alternatives for complex system applications where high reliability is required. Due to these characteristics, the application of the SC has been extended from simple systems such as electric motors to systems for generating electricity from renewable energy sources [19], [20], [21], [22]. These works demonstrated the efficiency and performance of the SC strategy in improving the characteristics of several systems and strategies, such as overcoming the problems and defects of both PI and DPC. In addition to improving the characteristics of both the synchronous machine and boost converter.

A new idea for SC was presented in [38], [39] in order to overcome the problems of the DPC strategy, where both SMC and terminal sliding surface were used for this purpose. The use of these strategies increased the robustness and performance of the SC strategy used to overcome the defects of DPC, and this is shown by the results obtained in the works [22], [23]. Ref. [24] proposes a SSMC to improve the effectiveness of the direct FOC of the AG-MRWP system using the PWM. In [25], the authors combined a super-twisting algorithm (STA) and SC to obtain a strategy characterized by robustness and high performance of AG control. In addition, the author has used a modified SVM to generate the RSC control pulses. A comparative study between the SC and STA controllers was carried out in [26]. This study was done in terms of complexity, ease of use, durability, current quality, response time, and ripple ratio. The simulation results showed the high performance of the SC compared to the STA.

Another technique that has been used in the field of electrical engineering, especially in the field of renewable energies, is no less important than the rest of the other methods. This method is called fractional calculus. Fractional calculus is a branch of calculus that is of great importance in improving the characteristics of systems. This method has been applied in several fields [27], [28], [29]. Due to the efficiency of this method in improving and increasing the advantages of the systems, this control was used to improve the quality of the energy generated from wind stations. In [30], fractional calculus is used to improve the field-oriented control(FOC) properties of an AG-based wind turbine. The use of fractional calculus significantly improved the quality of the current compared to the traditional strategy such as the FOC. However, the problem of *Ps* ripples remains, and the value of the THD of the current is rather high. A FOC for microgrids was presented in [31], where minimizing the ripples of *Ps* and current was the main aim of this work. An SMC based on fractional calculus is designed to control the AG-WP system [32]. In [33], the DPC based on the fractional-order SMC (FOSMC) is suggested to regulate the *Ps* and *Qs* of the AG-WP. Using the FOSMC increases DPC durability and somewhat overcomes the spawn system's drawbacks. But in the case of changing the system parameters, it is noted that the DPC-FOSMC is greatly affected as a result of the FOSMC being attached to the system parameters, which creates problems and this is undesirable. A terminal SMC based on adaptive FOC was proposed to control the RSC, where the performance of the designed strategy is compared with the DPC [34]. Compared to the DPC, this method is more sophisticated, making it more challenging to be implemented in practice. However, simulation results show the characteristic of this DPC in improving the quality of *Ps* and in reducing the value of ripples. In [35], the author has combined FOC and artificial intelligence technique to obtain a method that is more robust and has high advantages to reduce electrical current ripples from wind farms. In [36], the PI control was designed based on FOC with an intelligent PWM, where a reference rotor voltage was calculated based on the estimated *Ps*, rotor flux, *Qs*, and *Qs*/*Ps* error. The advantage of the proposed controller is durability with less power ripple compared to DPC, where the current quality is greatly improved. However, this negative strategy is represented by estimating each of the Ps and Qs, which makes defects in the case of changing the system parameters, is not desirable. Ref. [37] proposes a fractional-order PI-STA to control the *Ps* and *Qs* of the AG fed by a 2-level SVM. The *Ps* and *Qs* power of DFIG have been precisely regulated using a FOSMC based on a multi-objective gray wolf optimizer (MOGWO). The chattering amplitude has decreased and the system uncertainties have been addressed via the FOSMC-MOGWO controller [38]. The obtained simulation results prove the efficiency and performance of the MOGWO-based FOSMC controller to accurately track the *Ps* and *Qs* of the DFIG and minimize ripples, which is desirable. To enhance the performance of DFIG-WPs by increasing the PQ and supporting fault ride-through (FRT), fractional-order STA for dynamic voltage restorer was investigated [39]. Beside sincreasing FRT power and extracting the most power for DFIG-WP, optimal RPO-FOSMC based on a multi-objective grasshopper optimization algorithm was studied [40].

Through these works mentioned in this paper, these proposed techniques for controlling AG-WP differ in terms of the degree of complexity and ease of implementation, naturally from the perspective of the results. In addition, the problem of power fluctuations and the low quality of network current remain to be further studied and solved with better performances. Using nonlinear methods such as the SMC and passivity control increases the current quality and reduces the *Ps* fluctuations compared to the DPC. But the use of this strategy increases the complexity of the system, which is difficult to achieve experimentally. In this work, a control scheme that is simple, low in complexity, easy to implement, and robust compared to the DPC is proposed.

In this paper, a new nonlinear technique is presented based on the use of FOC and SC to increase the efficiency of the DPC of an AG-based MRWP system. The *Ps* and *Qs* are regulated using the fractional-order SC (FOSC). So FOSC is the main contribution in this paper, which was used to overcome the defects of the power generation system. This technique has advantages and characteristics such as simplicity, as it is considered one of the simplest controllers in the field of control. In addition, it contains a small number of parameters (only two), which facilitates the adjustment of the dynamic response of the system and facilitates the use of artificial intelligence theories such as genetic algorithms. The DPC-FOSC is used to calculate the generator rotor reference voltage. Accordingly, the main contributions of this work can be summarized in the following points: (1) Applying the proposed FOSC controller to increase the efficiency of the DPC of an AG-MRWP system, (2) Improving the performance of the AG-MRWP system through minimizing the THD and increase the efficiency, (3) Test the robustness of the proposed AG-MRWP through system parameter and wind speed (WS) variations.

The strategy proposed in this paper is different from other strategies proposed in published works such as [35], [36], [38]. In addition, the ratios of *Ps* ripples and SSE are extracted and it is shown that there is a significant improvement compared to the DPC. Moreover, the behavior of the DPC-FOSC is examined in the case of changing the generator parameters since changing the parameters may cause disturbance in the operation of the generating system. In DPC-FOSC, the reference value of the *Ps* is calculated using the maximum power point tracking (MPPT), making the *Ps* highly dependent on the WS. Three different tests are suggested to demonstrate the performance characteristics of the DPC-FOSC. To elaborate the work performed in this paper, the design, testing, and validation stages of the DPC-FOSC are shown in Figure 1.

This paper is organized as follows. Section II provides an overview of the generation system (MRWP system) proposed in this paper with its pros and cons. Section III explains the designed fractional-order synergetic control to control the AG power. The proposed DPC strategy based on a FOSC technique and the two-level PWM strategy, has been presented in section IV. Numerical simulation studies are presented in Section V. The conclusions and next work are given in Section VI.

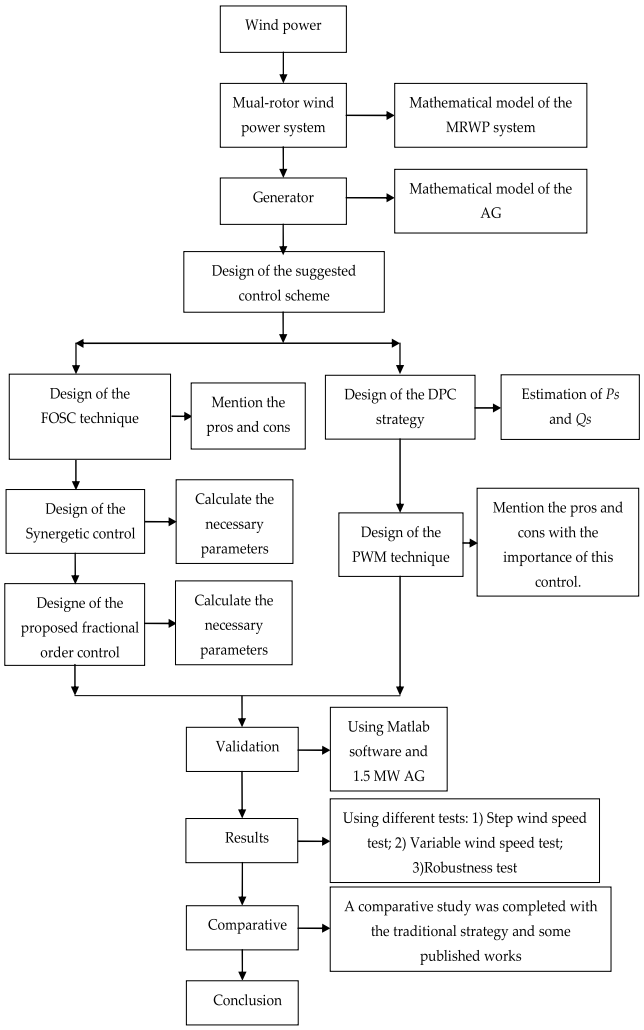

FIGURE 1. Diagram for proposed approach.

II. MRWP SYSTEM

Renewable energies are among the powers or means that are currently considered the most effective solutions to overcome global warming and avoid the use of traditional powers of producing electric energy such as gas. WP is the most widely used and least expensive type, as three-bladed turbines are mostly used to convert WP into mechanical power [33]. Figure 2 represents the system used in this paper to generate electricity from wind, as this system relies on MRWP. This system has the advantages of being easy to use, simple, and ecologically beneficial. This generation system comprises a generator (AG), two inverters, and an MRWP. These two inverters are used in this system to feed the rotor AG and control the rotational speed. The primary function of the first inverter, which is located on the grid side, is to convert alternating current to direct current. Also, a second inverter is used to convert direct current into alternating current. In the suggested MRWP system, MRWP is used to increase the value of the mechanical energy gained from the wind [30]. This mechanical energy is used to rotate the AG. This generator has several advantages, including ease of control, durability, low cost, low maintenance, and operation in variable WS conditions [10]. Moreover, The generator has two main parts, one is static and the other is a rotating part, these two parts can be expressed using the park transformation. Equation (1) represents the voltage of the rotor and the stator part of the AG, and Equation (2) represents the relationship that relates torque with rotational speed. The *Ps* and *Qs* of the AG is calculated according to Equation (3).

$$\begin{cases} V_{dr} = R_r I_{dr} - w_r \Psi_{qr} + \dfrac{d}{dt}\Psi_{dr} \\ V_{qr} = R_r I_{qr} + w_r \Psi_{dr} + \dfrac{d}{dt}\Psi_{qr} \\ V_{qs} = R_s I_{qs} + w_s \Psi_{ds} + \dfrac{d}{dt}\Psi_{qs} \\ V_{ds} = R_s I_{ds} - w_s \Psi_{qs} + \dfrac{d}{dt}\Psi_{sd} \\ \Psi_{dr} = L_r I_{dr} + M I_{ds} \\ \Psi_{qr} = M I_{qs} + L_r I_{qr} \\ \Psi_{qs} = M I_{qr} + L_s I_{qs} \\ \Psi_{ds} = L_s I_{ds} + M I_{dr} \end{cases} \tag{1}$$

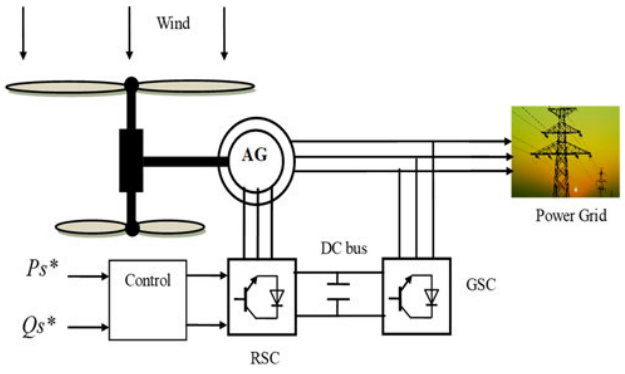

FIGURE 2. Block diagram of the MRWP system.

where, *Ls* and *Lr* are the stator and rotor inductances, *Vdr* and *Vqr* are the direct and quadrature rotor voltages, *Vds* and *Vqs* are the direct and quadrature stator voltages, *Ids* and *Iqs* are the direct and quadrature stator currents. The stator and rotor inductances are represented by *Ls* and *Lr*, respectively, and the magnetizing inductance is represented by *M*.

$$\begin{cases} P_s = 1.5 \times (V_{qs} \times I_{qs} + I_{ds} \times V_{ds}) \\ Q_s = 1.5 \times (-I_{qs} \times V_{ds} + V_{qs} \times I_{ds}) \end{cases} \tag{2}$$

where, Qs is the reactive power, Rr is the rotor resistance, Ps is the active power, and Rs is the stator resistance.

$$\begin{cases} T_e - T_r = J \times \dfrac{d\Omega}{dt} + f \times \Omega \\ T_e = 1.5\, p \times \dfrac{M}{L_s}(-\Psi_{sd} \times I_{rq} + \Psi_{sq} \times I_{rd}) \end{cases} \tag{3}$$

where, Te is the torque of the AG, J is the inertia, f is the viscous friction coefficient, Ω is the mechanical rotor speed, and T_r is the load torque.

In the proposed system for generating electric power, the MRWP is one of the most important elements or pillars of this system. This new wind turbine is one of the latest technologies that have appeared in recent years to overcome the disadvantages of the traditional wind turbine. This development added an auxiliary turbine to the conventional horizontal-axis turbine. Using this type of turbine significantly reduces the size of wind farms, which lowers the construction and electricity consumption costs [10]. In addition, the mechanical disturbances that the outdated technology had been diminished by this new technology. However, its drawbacks include increased manufacturing costs compared to traditional wind turbines and the control complexity of this new technology [27]. The usage of two wind turbines, each of varying size and power, located on the same axis, is essential to this novel technology. This new technology depends on using two wind turbines of different sizes and power, where they are assets on the same axis. The resulting torque is the sum of the torques of the two turbines together and the same for the resulting mechanical power [1]. The torque and power of MRWP can be expressed by Equation (4).

$$\begin{cases} T = T_2 + T_1 \\ P = P_1 + P_2 \end{cases} \tag{4}$$

where, T and P are the torque and mechanical power of the MRWP system, respectively; T_1 and T_2 are the torque of the secondary and main turbines, and P_1 and P_2 are the mechanical power of the secondary and main turbines.

The basic equation for the dynamics of a mechanical system on a generator rotor can be written by Equation (1).

$$\begin{cases} \left(\dfrac{J_1}{G_1^2} + \dfrac{J_2}{G_2^2} + J_g\right)\dfrac{d\Omega_g}{dt} + f_v\Omega_g = T_g - T_{em} \\ G_1 = \dfrac{r_1}{r_g} \\ G_2 = \dfrac{r_2}{r_g} \\ \dot{\theta}_2 = \dfrac{r_g}{r_2}\dot{\theta}_g \\ \dot{\theta}_1 = \dfrac{r_g}{r_1}\dot{\theta}_g \end{cases} \tag{5}$$

where, r_2 and r_1 are the dimensions of the two turbines in meters, J_1 and J_2 are the inertia of the secondary and main turbines, and J_g are the inertia of the generator.

The generator torque (T_g) can be written in terms of the main turbine torque (T_1) according to the following equation:

$$\begin{aligned} T_g - T_1 - d_g\dot{\theta}_g + d_1\dot{\theta}_1 =& J_g\ddot{\theta}_g - J_1\ddot{\theta}_1 + r_1K_{2g}\left[r_2\dot{\theta}_2 + r_g\theta_g\right] \\ &+ r_1d_{2g}\left[r_2\dot{\theta}_2 + r_1\dot{\theta}_1\right] \end{aligned} \tag{6}$$

where, $\dot{\theta}_2$ and $\dot{\theta}_1$ are the angular velocity of two turbines.

If friction in the gear system is neglected, the Equation (6) is written as follows:

$$T_g = J_g\ddot{\theta}_g - J_1\ddot{\theta}_1 - \frac{r_1}{r_2}J_2\ddot{\theta}_2 + T_1 + \frac{r_1}{r_2}T_2 \tag{7}$$

Equation (8) expresses the kinetic force (P_t) of the wind obtained through the main rotor with radius R_2. In addition to the power captured by the main rotor (P_{t2}) [22], [25].

$$\begin{cases} P_2 = \dfrac{1}{2}\rho\pi R_2^2 V_2^3 \\ P_{t2} = C_p\left(\lambda, \beta\right) P_2 \\ C_p\left(\lambda, \beta\right) = (0.5 - 0.167\,(\beta - 2)) \\ \sin\left(\dfrac{\pi\left(\lambda - 0.1\right)}{18.5 - 0.3\,(\beta - 2)}\right) \\ -0.0018\,(\beta - 3)\,(\beta - 2) \end{cases} \tag{8}$$

where, $\mathrm{Cp}(\lambda, \beta)$ is the coefficient of power, the $\mathrm{Cp}(\lambda, \beta)$ is very important and is related to the pitch angle (β) and λ, and ρ is the air density.

The secondary rotor speed ratio, speed, torque of the secondary rotor are given by [24]:

$$\begin{cases} \lambda_1 = \dfrac{\Omega_1 R_1}{V_1} \\ \Omega_1 = \dot{\theta}_1 \\ T_1 = \dfrac{\mathrm{C}_p\left(\beta, \lambda\right).\rho.\pi.V_1^3.R_1^2}{2\Omega_1} \end{cases} \tag{9}$$

The tip speed ratio, rotational speed, and aerodynamic torque developed by the main rotor are represented in Equation (10) [23], [25].

$$\begin{cases} \lambda_2 = \dfrac{\Omega_2 R_2}{V_2} \\ \Omega_2 = \dot{\theta}_2 \\ T_2 = \dfrac{\mathrm{C}_p\rho\pi V_2^3 R_2^2}{2\Omega_2} \end{cases} \tag{10}$$

where, λ_1 and λ_2 are the tip speed ratio of the secondary and main turbines, R_1 and R_2 are the blade radius of the secondary and main turbines. While Ω_1, and Ω_2 the mechanical speed of the secondary and main turbines.

In the MRWP system, each turbine has its wind speed, where the WS of the main turbine differs from the WS of the secondary turbine. To calculate the WS of the second turbine, Equation (9) is used, where this speed relates to the distance between the secondary and main turbine, which is estimated at 15 meters in this paper. Also, this speed is related to a constant ($\mathrm{C_T}$) of 0.90 [1], [27].

$$V_2 = V_1\left(1 - \frac{1 - \sqrt{(1 - C_T)}}{2}\left(1 + \frac{2x}{\sqrt{1 + 4x^2}}\right)\right) \tag{11}$$

where, C_T is the coefficient which characterized the reliability which is generally equal to 0.9 and x is the distance between the center of the second and first turbines ($x = 15$ m) [23], [25].

By analogy with the single-rotor wind turbine (SRWT) model, we can deduce the block diagram in Figure 3 which presents the speed control for maximizing the power extracted from a double-rotor wind system (DRWP) or MRWP. Equation (12) can be written that expresses the reference speed of the generator in terms of the speed of the main turbine. This reference speed is essential in determining the maximum value of energy that can be gained from the wind, as the reference value of speed is used to protect the turbine from strong winds.

$$\begin{cases} \Omega_g^* = G_2 \Omega_2^* \\ \Omega_2^* = \dfrac{\lambda_{opt} V_2}{R_2} \end{cases} \tag{12}$$

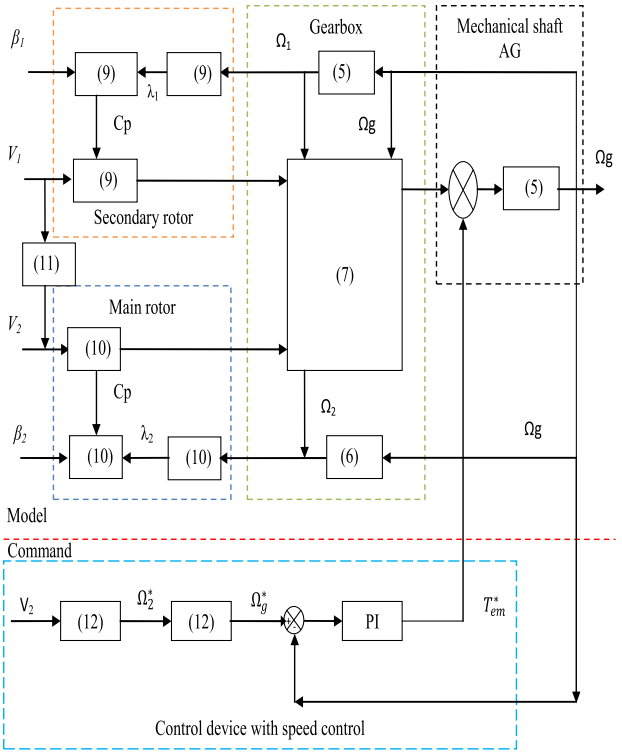

FIGURE 3. MPPT control with servo-control of the rotation speed of an DRWP.

In the literature, there are different regulation techniques that can be applied to control the rotational speed of an DRWP turbine (MRWP). In order to achieve this task, in this work, we applied a classic PI corrector for the MPPT control of an DRWP or MRWP.

In general, the objective of a control system is to minimize the difference $e(t)$ between the output of a system and a desired setpoint value. A proportional integrator type corrector is chosen to control the rotational speed of an DRWP turbine or MRWP. The structure of the speed controller is shown in Figure 4.

The closed-loop transfer function can be written in the following mathematical form:

$$\begin{cases} \Omega_g = H(s)\,\Omega_g^* + G(s).T_g \\ H(s) = \dfrac{K_p.s + K_i}{J_d.s^2 + \left(f_v + K_p\right).s + K_i} \\ G(s) = \dfrac{\dfrac{K_p.s + K_i}{s}}{J_d.s^2 + \left(f_v + K_p\right).s + K_i} \end{cases} \tag{13}$$

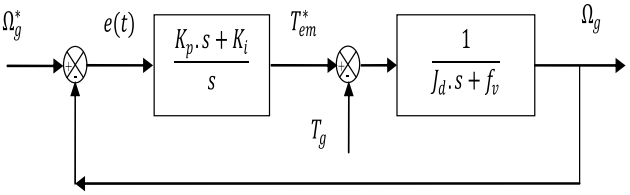

FIGURE 4. Scheme PI regulator block.

To reduce the effect of the disturbance (mechanical torque T_m), it is in our interest to choose a high value for the gain Kp. The other gain is chosen so as to have a 2nd order transfer function, having a natural pulsation and a damping coefficient, determined as follows:

$$\begin{cases} w_n = \sqrt{\dfrac{K_i}{J_d}} \\ \xi = \dfrac{f_v + J_d + K_p}{K_i} \dfrac{w_n}{2} \end{cases} \tag{14}$$

So, to impose a response time and a damping factor, we find:

$$\begin{cases} K_{i\Omega} = w_n^2 J_d \\ K_{p\Omega} = 2\xi w_n J_d - f_v \end{cases} \tag{15}$$

With: $J_d = (\frac{J_1}{G_1^2} + \frac{J_2}{G_2^2} + J_g)$

In Figure 5, simulation results are given for a 1.5 MW SRWP and a 1.5 MW DRWP using the wind speed profile of Moroccan City of Al Hoceima used in the works [9], [11], [37] and shown in Figure 3a. The mechanical energy generated by the two turbines is shown in Figure 3b, where it is noted that the energy generated by the DRWP turbine is greater than the energy generated by the SRWP, with the value of the generated energy changing according to the change in wind speed. At the time point of 1 second, the energy gained from wind reached 788.5 kW and 844 kW for SRWP and DRWP, respectively. In addition, the energy gained from wind reached 948.65 kW and 1.016 MW for both SRWP and DRWP, respectively, at the time point of 6.4 seconds. The largest value of the energy gained from the wind for the two turbines was at the time instant of 2.42 seconds, where the value reached 975.55 kW and 1044.9 kW for both SRWP and DRWP, respectively. Since the wind speed is variable, this causes the energy gained to change, as its lowest value at the moment of time takes 7.6 seconds. This value was 614.55 kW

and 705.31 kW for SRWP and DRWP, respectively. From the given values, it is clear that DRWP provides more incredible energy gained from wind than SRWP, which is desirable and important. On the other hand, the generator speed is shown in Figure 3c for the two turbines, where it is noted that the generator speed changes according to the change in wind speed and that the generator speed is greater in the case of using DRWP compared to the SRWP. At the time point of 4 seconds, the generator speed reached 1837.6 tr/min and 1968.32 tr/min for SRWP and DRWP, respectively. The largest value of the generator speed was at 2.42 seconds, reaching 2329 tr/min and 2494.5 tr/min for SRWP and DRWP, respectively. At the time point of 7.60 seconds, the generator speed reached its lowest value for the two turbines, reaching 1571.684 tr/min and 1683.58 tr/min for SRWP and DRWP, respectively. It is noted from these values that the speed of the generator is greater if a DRWP is used, and this is a result of the fact that the energy gained from the wind is greater in a DRWP. As is known, rotational speed is largely related to energy or torque, as the greater the energy, the greater the rotational speed.

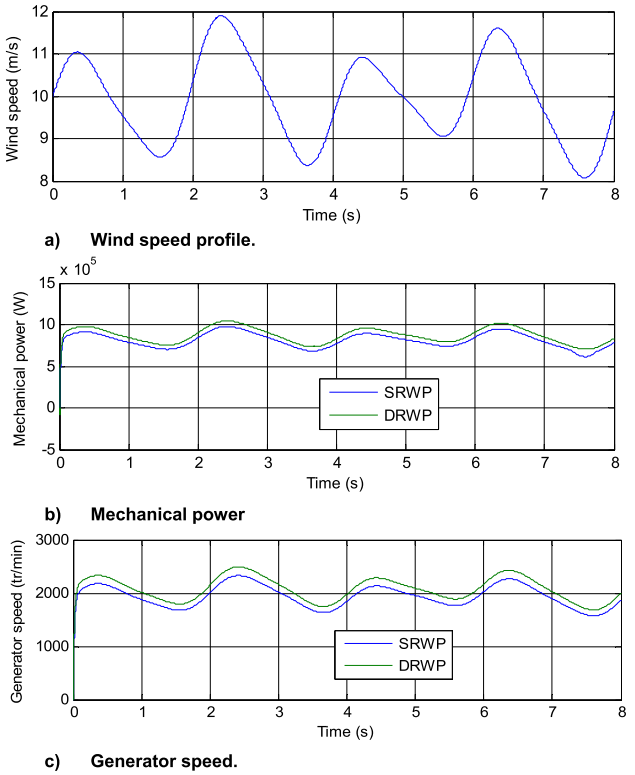

FIGURE 5. DRWP turbine simulation results.

III. DESIGN OF THE FOSC CONTROLLER

SC is a simple and uncomplicated nonlinear control, where this technique is based on the analytical design of aggregated controllers (ADAR). The main advantage of the SC is that it maps the original system of equations to a dynamical system such that (2) the attracting point is located at the solution of the original system, (1) any trajectory in the state space of the system ends in an attractive point and (3) the rate at which the dynamical system moves towards the attracting point is controllable. It can be said that the SC is the theory of synthesis of closed-loop control systems based on the formation of coherent cooperative processes in systems of different natures. In general, the SC is a control that has effectiveness and high performance to control nonlinear systems compared to traditional strategies, as it depends on the fixed principle in controlling the sliding situation, but it did not have a defect, which is represented in the chattering phenomenon. Despite all these advantages mentioned, there are still negatives that limit its spread, as the problem of low performance remains in the event of a change in the system parameters with the presence of ripples and a decrease in the quality of the current, and this is not desirable in the field of control.

In this section, two different strategies are combined in principle to improve the performance of the SC, the first strategy is SC and the second technique is fractional calculus to obtain a robust strategy. The FOSC is designed to overcome the disadvantages of the SC and give a new robust nonlinear technique. The FOSC is the first time presented as a work to control the *Ps* and *Qs* of an AG- MRWP system. Moreover, durability and simplicity are two of the biggest advantages of this proposed controller. As it is known, the SC is among the most simple and easy-to-implement nonlinear methods, as it can be applied to complex systems easily compared to the SMC [22]. The SC is widely used to control nonlinear systems. SC is a combination of modern mathematics and synergy [23]. This technique has multiple advantages such as durability, simplicity, and stability. Also, this method is characterized by high robustness against modeling inaccuracies and internal parameter disturbances [22], [24]. This method can minimize the order of the control system and can reduce the problem of chattering compared to the SMC [25]. In fact, the SC is more suitable for digital control than any other field. SC can be expressed by the following Equation [22], [25]:

$$T \cdot \dot{\varphi}(x) + \varphi(x) = 0 \tag{16}$$

where $T > 0$ represents the convergence speed and φ is the macro-variabledenoted by:

$$\varphi(x) = 0 \tag{17}$$

The derivation of Equation (17) is given by Equation (18):

$$\dot{\varphi} = \frac{d\varphi}{dx}\dot{x} \tag{18}$$

Taking into account the chains of differentiation which is given by:

$$T\frac{d\varphi(x,t)}{dt} = \frac{d\varphi}{dt}\frac{dx(t)}{dt} \tag{19}$$

Based on Equation (16), it can be inferred that the condition T > 0 ensures the satisfaction of Equation (20), hence enabling the attainment of the manifold described in Equation (17).

$$\begin{cases} \varphi_i > 0, \varphi_i < 0 \Rightarrow \varphi_i \longrightarrow 0 \\ \varphi_i < 0, \varphi_i > 0 \Rightarrow \varphi_i \longrightarrow 0 \end{cases} \tag{20}$$

Equation (21) expresses the mathematical solution to Equation (16), where for $t = 0$, $\phi(t) = S_0$. If $t = T$, in this case, $\phi(t) = S_0 \times e$, which is an exponential function.

$$\varphi(t) = \varphi_0 \cdot e^{t/T} \tag{21}$$

where for $t = 0$, $\varphi(0) = \varphi_0$, and for $t = T$, $\varphi(T) = \varphi_0 \cdot e$.

The SC is known to be a stable method, and Lyapunov theory can be used to check stability. Equation (22) represents the Lyapunov function used in this part to check the stability of the SC:

$$V = \frac{1}{2}\phi(\varphi)^2 \tag{22}$$

To study stability, the derivation of the Lyapunov function must be calculated since the derivation of this function can be expressed by Equation (23).

$$\dot{V} = \dot{\phi}(\varphi) \cdot \phi(\varphi) \tag{23}$$

As is known, for the strategy to be stable, the derivative $\dot{V}$ must be less than 0. So, based on the above relations, in this case we can write:

$$\dot{V} = -\frac{1}{K}\phi^2(\varphi) \leq 0 \tag{24}$$

Therefore, SC technique stability is guaranteed due to the negative derivative of the Lyapunov function.

There are several drawbacks present in the SC, as the use of this technique in controlling electrical machines leads to the presence of ripples in the current and torque, and in addition, reduces its durability [10]. To increase the durability and efficiency of the SC, FOC is used to reduce and overcome these aforementioned problems. However, FOC is one of the oldest solutions that has been proposed [33], [34]. It is a mathematical solution that has several characteristics and advantages that distinguish it from other solutions. This technique has been used in several fields, such as electronics and control [35], [36], [37], [38], [39]. Using this technique significantly improves system efficiency.

FOSC is a new nonlinear technique, which is designed for the first time in this work to improve the current quality and raise the efficiency of the DPC of the AG-MRWP. This strategy is a combination of the advantages of both SC and the advantages of fractional calculus, where robustness and simplicity of the algorithm are among the features of this new nonlinear method. However, the FOSC is a modification of the SC technique, where the FOC is used to increase the efficiency and characteristic of the SC. The FOSC can be expressed by Equation (24). Equation (25) is the mathematical form of the proposed FOSC controller. This mathematical model was obtained based on Equation (16) with the addition of a special factional calculus to it. This mathematical model has a unique feature: it plays the role of two different controllers depending on the value of the gain μ.

$$u(t) = (T \cdot \dot{\varphi}(x) + \varphi(x))^{\mu} \tag{25}$$

where μ is a positive gain expressing the FOC. For example, if $\mu = 1$, the FOSC becomes a SC. To use the suggested control, the condition $\mu > 0$ must be met. On the other hand, μ is used to modify the response of the FOSC in a way that allows obtaining high efficiency and greatly reducing the current and torque fluctuations of the AG-MRWP system.

Figure 6 shows the FOSC to overcome the drawback of the DPC. From this figure, the FOSC is not complicated, easily accomplished, and simple structure compared to other nonlinear strategies such as SMC and BC. As it is known the SC and FOC are known for their high performance and their insensitivity to the change of system parameters, which makes the FOSC more robust and characterized by high efficiency in improving the defects of any system.

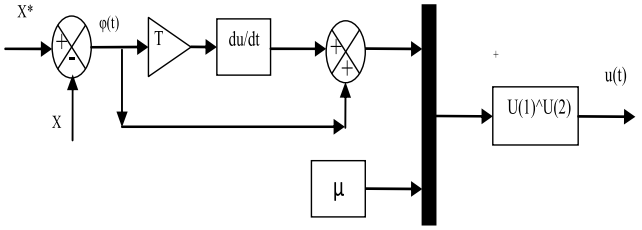

FIGURE 6. Proposed FOSC technique.

IV. PROPOSED DPC-FOSC STRATEGY

DPC has been used to control the WP generation systems for years due to its ease of implementation and simplicity [1], [2]. This technique depends on regulating the *Ps* and *Qs* by choosing the optimal voltage vector without measuring the *Qs*, torque or *Ps* [4], [5]. In this technique, only current and voltage are measured. These measurements are used to estimate both the *Qs* and *Ps*. Compared to the FOC strategy, the DPC offers a fast dynamic response [21], [22]. This method has several disadvantages, including the low quality of the current (high THD value) and fluctuations at the level of *Ps* and *Qs* [10], [11], [12], [13]. Also, if system parameters change, this method is greatly affected due to the use of traditional HCs. To overcome these shortcomings and improve the efficiency of the DPC, it is suggested to use the method proposed in Section III, which is the FOSC shown in Figure 6.

The DPC based on FOSC techniques proposed in this section of the paper is a development and modification of both the DPC and DPC-SC. The DPC-FOSC with MPPT strategy is an evolution of the DPC, in which HCs and ST are eliminated and replaced by two FOSC algorithms and PWM, respectively. This strategy is used to control the RSC to reduce power ripples and increase the current quality. In addition, the estimation of both *Ps* and *Qs* is used in this new strategy, which affects this strategy in case of changing the values of the resistors (R_s and R_r). The use of the FOSC makes the DPC more robust and characterized by high performance compared to the DPC and this is shown by the results obtained in Section V. Also, this technique is easy to implement and inexpensive, and the dynamic response can be easily tuned due to a small number of parameters, which

is good. Figure 7 represents the DPC-FOSC for controlling the AG-MRWP system, where simplicity is one of the main features of this technique. As seen, the reference voltage vectors in the dq frame ($V_{rd}{}^*$ and $V_{qr}{}^*$) are transferred to the rotor stationary frame ($\alpha_r\beta_r$) and then are fed to the PWM. $\varepsilon_{Ps}= Ps^*-Ps$ and $\varepsilon_{Qs}=Qs^*-Qs$ are the power variations in one sample time, Qs and Ps are instantaneous Qs and Ps, where Qs^* and Ps^* are the desired power set points.

In this control, two FOSC techniques are used to regulate the Qs and Ps. However, PWM is used to control the rotor inverter. This DPC-FOSC is different from the papers [5], [9], [10], [27] in terms of the type of turbine used, the power of the AG, and the type of controller used.

The DPC-FOSC depends on regulating the Qs and Ps directly by using two FOSC techniques, without measuring the Ps, flux (rotor and stator), and AG speed, to obtain the required Ps and Qs. In this technique, only voltage and current are measured. These measurements are used to estimate the rotor and stator fluxes, where the estimated values are used to calculate both Ps, and Qs of the AG-MRWP.

To estimate the Ps and Qs, we first need to estimate the stator and rotor fluxes, which are estimated according to Equation (26).

$$\begin{cases} \Psi_{r\alpha} = \int_0^t (V_r - R_r \times i_{r\alpha})dt \\ \Psi_{r\beta} = \int_0^t (V_r - R_r \times i_{r\beta})dt \\ \Psi_{s\alpha} = \int_0^t (V_s - R_s \times i_{s\alpha})dt \\ \Psi_{s\beta} = \int_0^t (V_s - R_s \times i_{s\beta})dt \end{cases} \tag{26}$$

With:

$$\begin{cases} |\Psi_r| = \sqrt{\left(\Psi_{r\beta}^2 + \Psi_{r\alpha}^2\right)} \\ |\Psi_s| = \sqrt{\left(\Psi_{s\beta}^2 + \Psi_{s\alpha}^2\right)} \end{cases} \tag{27}$$

where, t is the time, Vr and Vs are the rotor and stator voltages, Ψ_r and Ψ_s are the rotor and stator fluxes, and Rr is the rotor resistance.

Equation (28) represents the relationship between voltage (stator and rotor) and flux (stator and rotor). This relationship can be used to calculate rotor and stator fluxes from the rotor and stator voltages.

$$\begin{cases} \left|\bar{V}_r\right| = \left|\bar{\Psi}_r\right| \times w_r \\ \left|\bar{V}_s\right| = \left|\bar{\Psi}_s\right| \times w_s \end{cases} \tag{28}$$

To estimate the Qs and Ps in this method, Equation (29) is used, where these estimated values are used to calculate the error in the Qs and Ps (ε_{Ps} and ε_{Qs}).

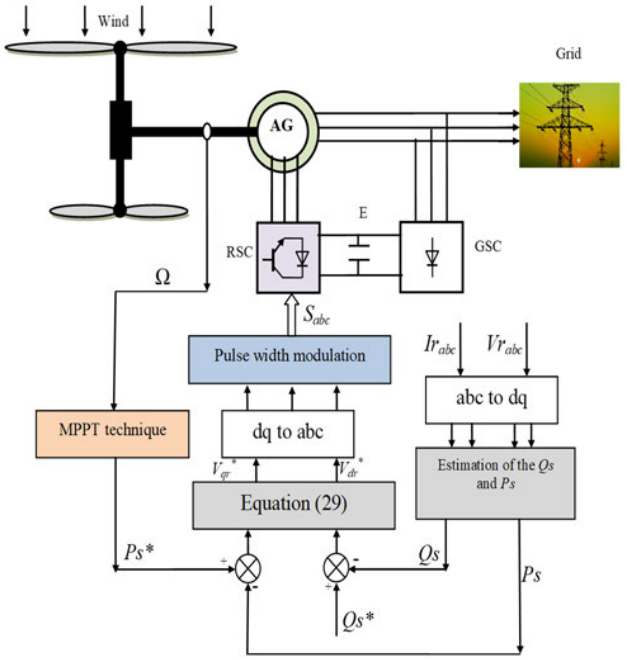

FIGURE 7. Proposed DPC-FOSC technique of AG-MRWP system.

$$\begin{cases} Q_s = -\frac{3}{2}\left(\frac{V_s}{\sigma \times L_s} \times \Psi_{\beta r} - \frac{V_s \times L_m}{\sigma \times L_r \times L_s}\right) \\ P_s = -\frac{3}{2} V_s \times \Psi_{r\beta} \times \frac{L_m}{\sigma \times L_r \times L_s} \end{cases} \tag{29}$$

where, $\sigma = 1 - \frac{M^2}{L_s L_r}$.

From Figure 3, the FOSC is used for calculating the reference values of both the quadrature and direct rotor voltage (V_{qr}^* and V_{dr}^*). Accordingly, these reference values are calculated according to Equation (30). It is concluded from Equation (30) that the Ps variation is regulated using the q-axis rotor voltage, while Qs is controlled via the d-axis rotor voltage

$$\begin{cases} V_{qr}^* = (T \cdot \dot{\varepsilon}_{Ps} + \varepsilon_{Ps})^{\mu} \\ V_{dr}^* = (T \cdot \dot{\varepsilon}_{Qs} + \varepsilon_{Qs})^{\mu} \end{cases} \tag{30}$$

where, ε_{Qs} and ε_{Ps} are the Ps and Qs errors, and μ is the fractional calculus ($\mu \neq 0$), which can take both negative and positive values.

If the value of μ is 1, the DPC-FOSC becomes the DPC-SC, and this is a positive thing for the DPC-FOSC because it is possible to switch from one controller to another by changing only the value of μ. Equation (31) represents the Ps and Qs errors:

$$\begin{cases} e_{Ps} = P_s^* - P_s \\ e_{Qs} = Q_s^* - Q_s \end{cases} \tag{31}$$

The MPPT is used to calculate the value of Ps^* (the reference value), where this value relates to the WS. In addition, the value of Qs^* is set at 0 VAR. Finally, Figure 8 represents the FOSC in Equation (30) for the Ps and Qs of the AG-based MRWP system.

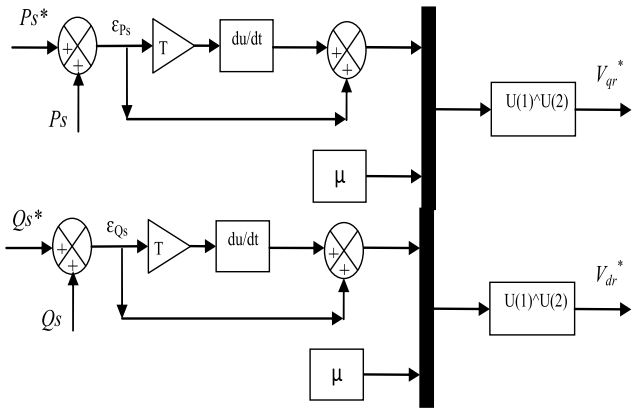

FIGURE 8. Proposed FOSC active and reactive power controllers.

V. RESULTS

Simulation tests of the DPC-FOSC applied to AG driven by a MRWP were performed under Matlab software, the simulation scheme is presented in Figure 7. This work was carried out using two different behaviors of WS, the first represented a stepping behavior and the second represented a random behavior, which allows studying different modes of operation of AG.

The results obtained from the DPC-FOSC are compared with those obtained from the DPC-PI, where they are compared between these controls in terms of SSE and the ratios of ripple reduction torque, *Qs*, and current. Also, the comparison is in terms of the THD of the current. The parameters of the AG with a power of 1.5 MW are as follows: $R_s = 0.012\ \Omega$, 380/696 V, $L_r = 0.0136$ H, $J = 1000$ kg.m^2, $L_m = 0.0135$ H, $R_r = 0.021\ \Omega$, fs=50 Hz, $L_s = 0.0137$ H, $p = 2$, and $f_r = 0.0024$ Nm/s.

A. THE FIRST TEST

The first test is to study the effectiveness of the DPC-FOSC in comparison with the behavior of the DPC-PI in the case of step WS, where the results obtained are shown in Figure 9. Figure 9 represents the *Ps*, current, torque, and *Qs* of both strategies. The *Ps* evolution depends on the mechanical speed and follows its reference (Ps^*) very well, as presented in Figure 9c. This ensures optimal power extraction. Its negative sign indicates the generator's operation. Therefore, the AG always supplies the AC grid with its stator.

The *Qs* also follow its reference (Qs^*) with a constant value of 0 VAR with low ripples for the DPC-FOSC, as shown in Figure 9d. In addition, the Qs value is not related to the WS, as it remains constant throughout the simulation.

The torque evolution is shown in Figure 9a, where it is noted that the shape of the torque is related to the profile of the *Ps,* and its value is affected by the WS with a preference for the DPC-FOSC in terms of dynamic response and SSE. The current takes the form of a sinusoidal, and its value is related to the *Ps*, where the frequency is 50 Hz, as shown in Figure 9b. The obtained currents are fed directly into the network without any filters.

The THD of the obtained current is shown in Figures 9f and 9e for both techniques. The THD for the current of the DPC-FOSC was 0.13% and for the DPC-PI strategy was 0.94%.Through these values, the proposed DPC-FOSC improved the current quality significantly and the percentage of reduction of THD value was about 86.17% compared to the DPC-PI.

The amplitude of the fundamental current signal is greater in the case of the DPC-FOSC (1889 A) compared to the traditional control, where the value of the amplitude is 1888 A, which we can say that the DPC-FOSC is much better than the DPC-PI.

Figure 10 represents the ripples for the *Ps*, current, torque, and *Qs* of the two techniques. Also, the ripple values are listed in Table 1. Through Table 1 and Figure 10, the DPC-FOSC has excellently minimized the current, *Qs*, torque, and *Ps* ripples compared to the DPC-PI, where the minimization ratios were about 93.72%, 85%, 72.50%, and 80% for the *Qs*, torque, *Ps*, and current, respectively.

Table 2 represents the ratios and values of the SSE, overshoot, and response time of *Ps* and *Qs* for the two methods in the first test. The DPC-FOSC demonstrated superior performance in terms of SSE value as compared to the DPC-PI, as seen by the consistently low valuess.. And accordingly, the DPC-FOSC reduced SSE by rates estimated at 94.55% and 93.72% for each of the *Ps* and *Qs*, respectively. On the other hand, the DPC-FOSC reduced the overshoot value for both the *Ps* and *Qs* and this was in high proportions, as the minimization rates were estimated at 85% and 98.59% for each of the *Ps* and *Qs*, respectively (Table 2). However, the DPC-FOSC provided unsatisfactory results in terms of response time for *Ps* and *Qs*, where the DPC-PI gave a batter response time value compared to the DPC-FOSC, and the ratios were estimated at 88.14% and 99.64% for both *Ps* and *Qs*, respectively, compared to the DPC-FOSC.

TABLE 1. Ratios and values of ripples in the first test case.

	Qs (VAR)	*Te* (N.m)	*Ps* (W)	*Ias* (A)
DPC-PI	66400	200	600000	30
DPC-FOSC	4170	30	165000	6
Ratios	93.72%	85%	72.50%	80%

B. THE SECOND TEST

In this test, the behaviour of the DPC-FOSC is studied compared to the DPC-PI in the case of variable WS of Morocco City of Al Hoceima (Figure 11), where the results obtained are shown in Figure 12. Through Figures 12c and 12d, the *Ps* and *Qs* track the references (Ps^* and Qs^*) well with

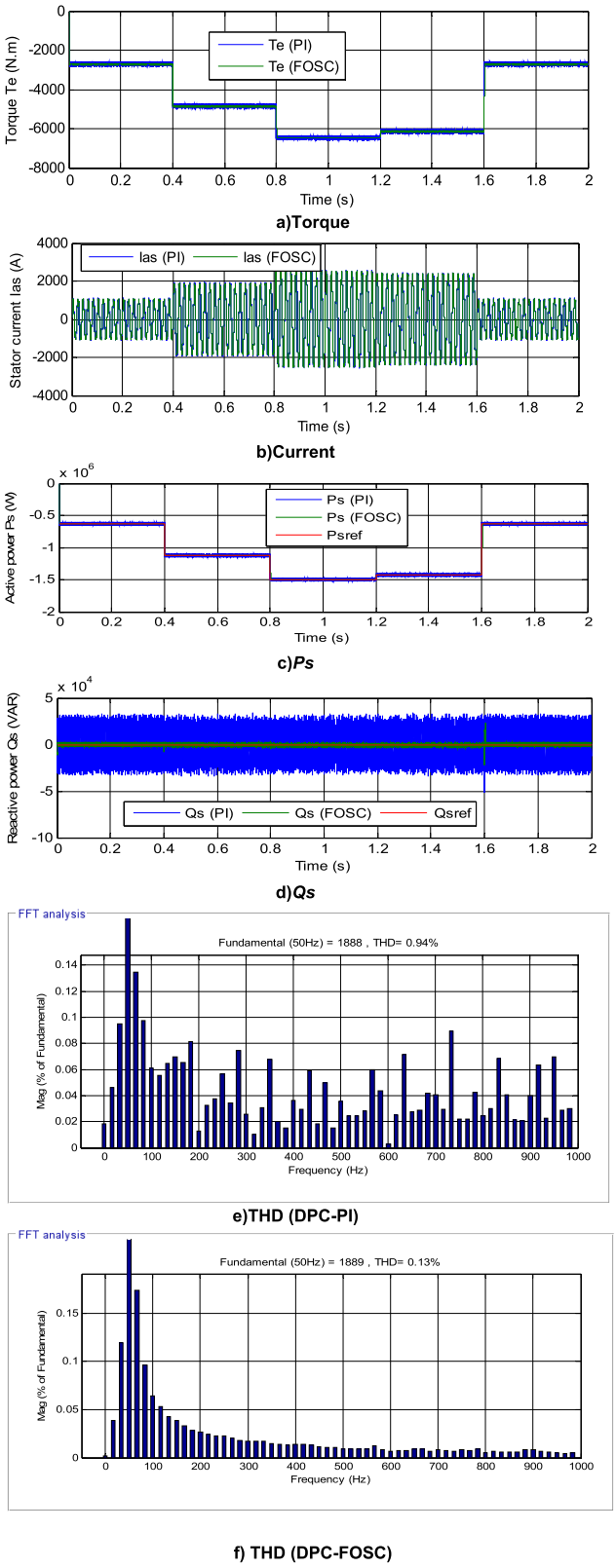

FIGURE 9. Results of the first test.

preference to the DPC-FOSC compared to the DPC-PI in dynamic response and SSE, where the *Qs* remains constant and equal to the value 0 VAR, the form of the development

TABLE 2. Ratios and values of the overshoot, SSE, and response time in the first test case.

		Ps (W)	*Qs* (VAR)
DPC-PI	Overshoot	6000	5537.8
	SSE	31200	33200
	Response time	0.78ms	0.0231 ms
DPC-FOSC	Overshoot	900	77.75
	SSE	1700	2085
	Response time	6.58 ms	6.57 ms
Ratios	Overshoot	85%	98.59%
	SSE	94.55%	93.72%
	Response time	88.14%	99.64%

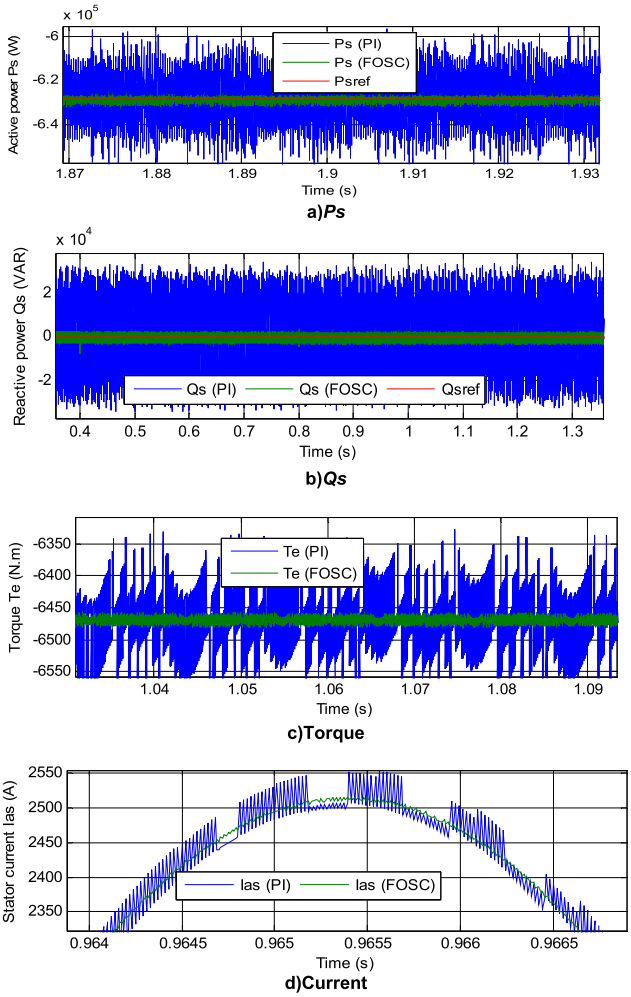

FIGURE 10. Zoom in the Qs, current, torque, and Ps (First test).

of the *Ps* takes the form of WS with the presence of ripples. In addition, the *Ps* takes negative values, indicating the AG operation.

The torque evolution depends on the *Ps*, as presented in Figure 12a. From Figure 12a, it can be said that the torque value is related to the value of the *Ps*. An increase in the value of the *Ps* leads to an increase in the value of both current and

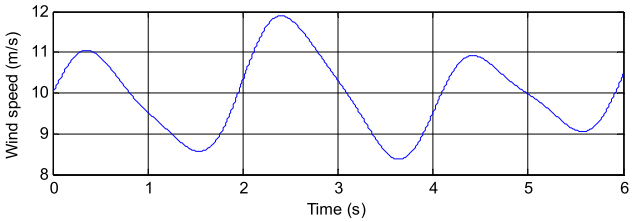

FIGURE 11. WS profile.

TABLE 3. Ratios and values of the ripples in the second test case.

	Qs (VAR)	*Te* (N.m)	*Ps* (W)	*Ias* (A)
DPC-PI	67000	275	603000	60
DPC-FOSC	5360	18	5000	7
Ratios	92%	93.45%	99.17%	88.33%

torque, but in the case of a decrease in the value of the *Ps* leads to a reduction in the value of torque.

The evolution of the generated current (*Isa*) had a sinusoidal form with a constant frequency (50 Hz), as presented in Figure 12b. The value of this current is related to the change in WS, where the shape of the current change is the same as the shape of the change in both the WS and the *Ps*. Figures 12e and 12f represent the THD values of the current for both DPC-PI and DPC-FOSC strategies, respectively. The DPC-FOSC gave a lower value for THD for the current compared to the DPC-PI, where the value of THD is 0.16% for the DPC-FOSC and 0.77% for the DPC-PI, which makes the reduction ratio to be about 79.22%. Through this ratio, it can be said that the DPC-FOSC has greatly improved the quality of the current compared to the DPC-PI. The amplitude of the fundamental of the current signal for the DPC and DPC-FOSC is 2292 A and 2293 A, respectively. With these values, the DPC-FOSC provided a better value and this is desirable. The torque, *Ps*, current, and *Qs* zooms are presented in Figure 13. From this figure, it can be seen that the DPC-FOSC presented fewer fluctuations compared to the DPC-PI. The values and ratios of the reduction of these ripples are shown in Table 3. Through this table, the DPC-FOSC reduces ripples by excellent rates, estimated at 99.17%, 88.33%, 92%, and 93.45% for each of the *Ps*, current, *Qs,* and torque, respectively.

The numerical results of this test are represented in Table 4, as this table represents the values and percentages of reduction in response time, overshoot, and SSE of Ps and Qs for both techniques of AG-MRWP. So, it can be seen from Table 4 that DPC-FOSC significantly reduced overshoot forces compared to DPC-PI, where the reduction rates were estimated at 64% and 93.02% for each of the *Ps* and *Qs*, respectively. On the other hand, the DPC-FOSC provided unsatisfactory results in terms of the response time of the powers, where the values and ratios of reduction are represented in Table 4. The DPC-PI reduced the value of response time with reduction rates that were 90.90% and 99.47% for each of the *Ps* and *Qs*, respectively, compared to the DPC-FOSC. Also, the SSE value of the *Qs* and *Ps* are reduced by DPC-FOSC compared to DPC-PI. Through Table 4, the DPC-FOSC improved the SSE values for both the *Ps* and *Qs*, as the reduction ratio was estimated at about 94.73% and 92% for each of the *Ps* and *Qs*, respectively.

TABLE 4. Ratios and values of the overshoot, SSE, and response time in the second test case.

		Ps (W)	*Qs* (VAR)
DPC-PI	**Overshoot**	10000	10900
	SSE	32300	33500
	Response time	0.0232 ms	0.4031 ms
DPC-FOSC	**Overshoot**	3600	760
	SSE	1700	2680
	Response time	4.386 ms	4.43 ms
Ratios	**Overshoot**	64%	93.02%
	SSE	94.73%	92%
	Response time	99.47%	90.90%

C. THE THIRD TEST

In this test, the characteristic of the DPC-FOSC is studied in the case of changing the generator parameters compared to the DPC-PI, whereby *Rs*, *Ls*, *Lm*, *Rr*, and *Lr* are changed to new values (Table 5). The WS used is the same as represented in Figure 11. Figure 14 represents the results of this test. Despite changing the parameters of the generator, both the *Qs* and *Ps* follow the references (Qs^* and Ps^*) well with an advantage to the DPC-FOSC in terms of ripples, dynamic response, and steady-state performance compared to the DPC-PI (Figures 14c and 14d). In addition, the *Qs* remain equal to the value 0 VAR, and the development of the *Ps* remains largely related to the WS despite the change in the parameters of the system.

Figures 14a and 14b represent the torque and current, respectively. Similar to the evolution of *Ps* and current, the torque evolution also exhibits considerable oscillations at the level of the DPC-PI approach in comparison to the DPC-FOSC. The latter minimized the THD of the current compared to the DPC-PI by an estimated ratio of 87.34% (Figures 14e and 14f). Through this ratio, it can be concluded that the DPC-FOSC outperforms the DPC-PI and is more durable when it comes to enhancing the quality of the current despite changes in AG characteristics. The amplitude of the fundamental of the current signal for the DPC-PI and DPC-FOSC is 2292 A and 2297 A respectively. With these values, the DPC-FOSC provided a better value and this is desirable.

Figure 15 shows the zooms in the *Ps*, torque, *Qs*, and current of both techniques. From this figure and Table 6,

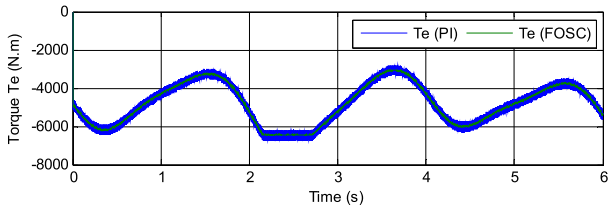

a)Torque

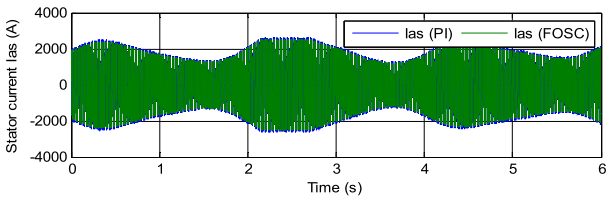

b)Stator current

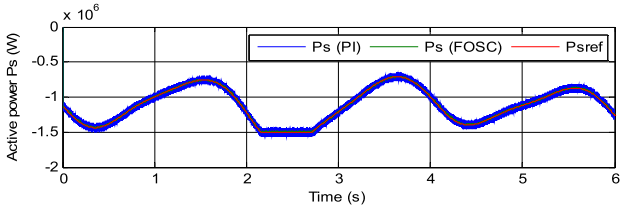

c)*Ps*

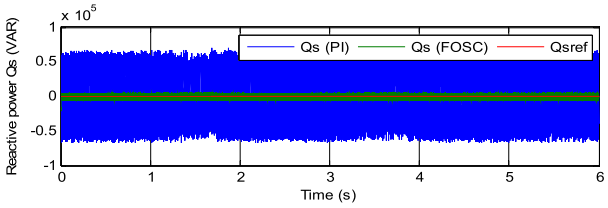

d)*Qs*

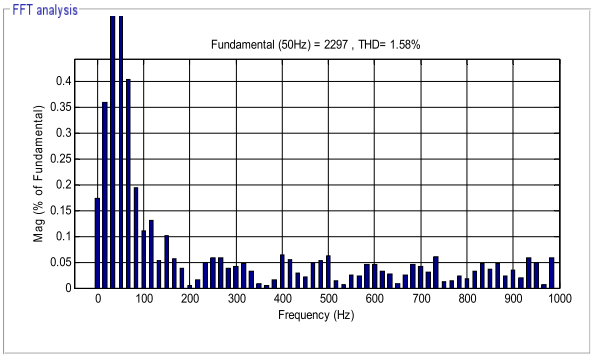

e)THD (DPC-PI)

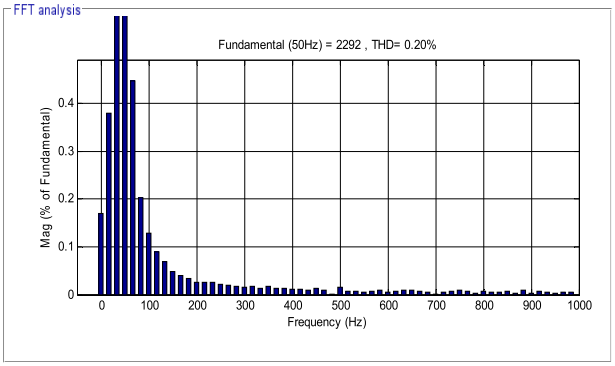

f) THD (DPC-FOSC)

FIGURE 12. Results of the second test.

it is noticed that the DPC-FOSC is not affected much by the change of system parameters compared to the DPC-PI due to the use of the FOSC. Also, it is noted that the DPC-FOSC minimized the ripples by 93.19%, 96%, 91.66%, and 92.81% for each of the *Qs*, torque, *Ps*, and current, respectively. These results make the DPC-FOSC one of the best strategies that can be suggested for controlling electrical machines.

TABLE 5. variable parameter values.

	Rs	*Rr*	*Ls*	*Lm*	*Lr*
Old values	0.012 Ω	0.021 Ω	0.0137 H	0.0135 H	0.0136 H
New Values	0.024 Ω	0.042 Ω	0.00685 H	0.00675 H	0.0068 H

Table 6 represents the numerical results for answer time, overshoot, SSE of Ps and Qs for both techniques in third test. From this table, the DPC-FOSC minimized the value of

TABLE 6. Ratios and values of the ripples in the third test case.

	Q_s(VAR)	T_e(N.m)	P_s (W)	I_{as} (A)
DPC-PI	133700	500	120000	160
DPC-FOSC	9098	20	10000	11.50
Ratios	93.19%	96%	91.66%	92.81%

the SSE for the *Ps* and *Qs* compared to the DPC-PI, where the reduction ratios are estimated by 88.32% and 62.30% for the *Ps* and *Qs*, respectively. On the other hand, the values and percentages of exceeding the limit value for both *Ps* and *Qs* are better when using DPC-FOSC compared to DPC-PI. So, the DPC-FOSC strategy reduced the overshoot value by 97.28 and 92.75 percent for Qs and Ps, respectively, compared to DPC-PI. These percentages indicate the high efficiency of the proposed control. However, the DPC-FOSC strategy provided unsatisfactory results with regard to the answer time for both *Qs* and *Ps* compared to DPC-PI,

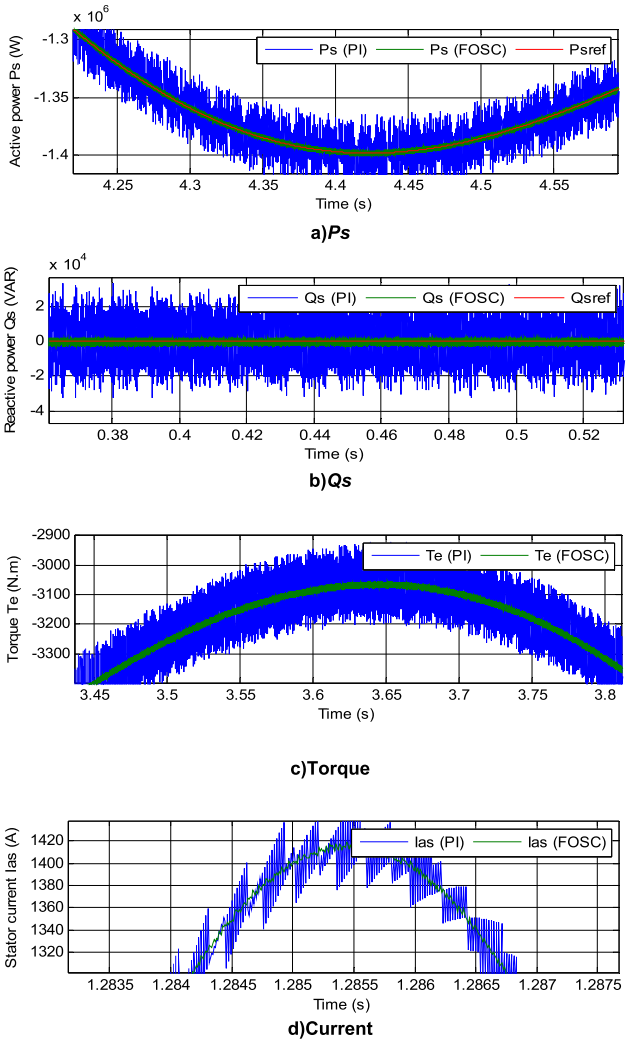

FIGURE 13. Zoom in the current, reactive power, torque, and Ps (Second test).

as the DPC-PI strategy reduced the answer time by percentages estimated at 98.61% and 99.25% for *Qs* and *Ps*, respectively.

TABLE 7. Ratios and values of the overshoot, SSE, and response time in the third test case.

		Ps (W)	*Qs* (VAR)
DPC-PI	Overshoot	2760	5537.778
	SSE	54800	66850
	Response time	0.0432 ms	0.0231 ms
DPC-FOSC	Overshoot	200	150.50
	SSE	6400	4549
	Response time	3.12 ms	3.09 ms
Ratios	Overshoot	92.75%	97.28%
	SSE	88.32%	62.30%
	Response time	98.61%	99.25%

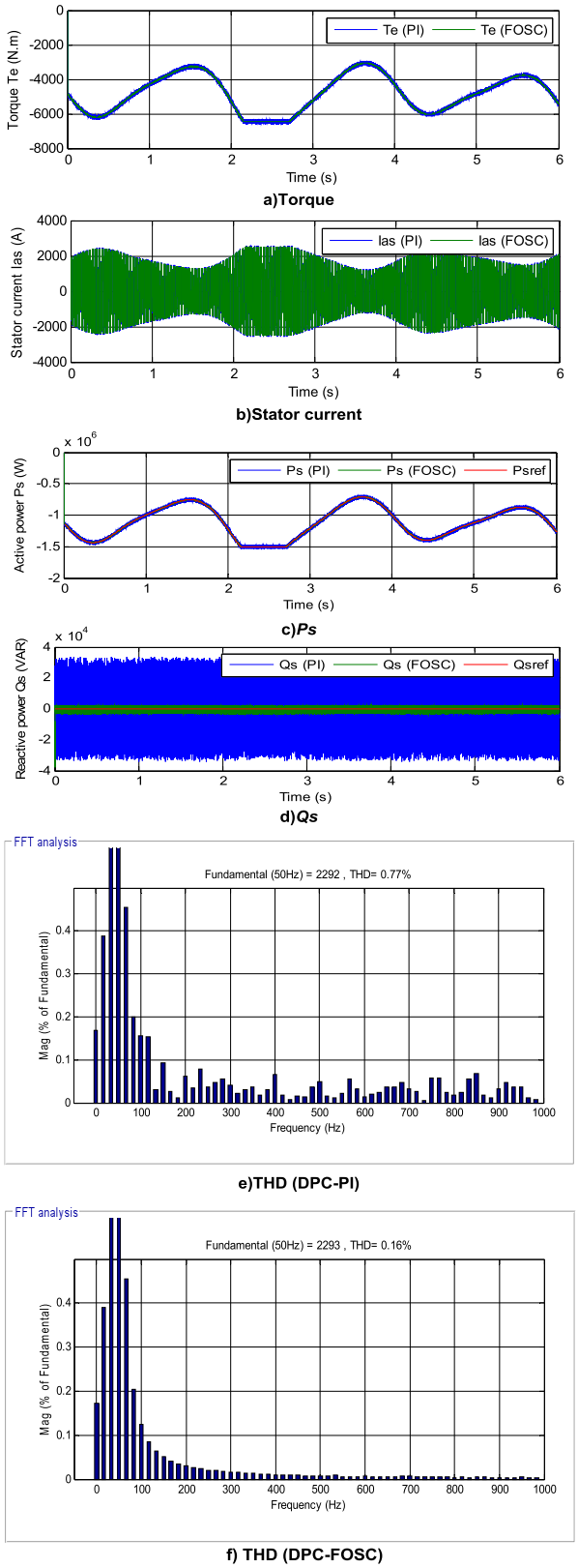

FIGURE 14. Results of the third test.

Finally, the DPC-FOSC is compared with some published strategies in terms of the THD of the current. The results are recorded in Table 8, where the DPC-FOSC improved

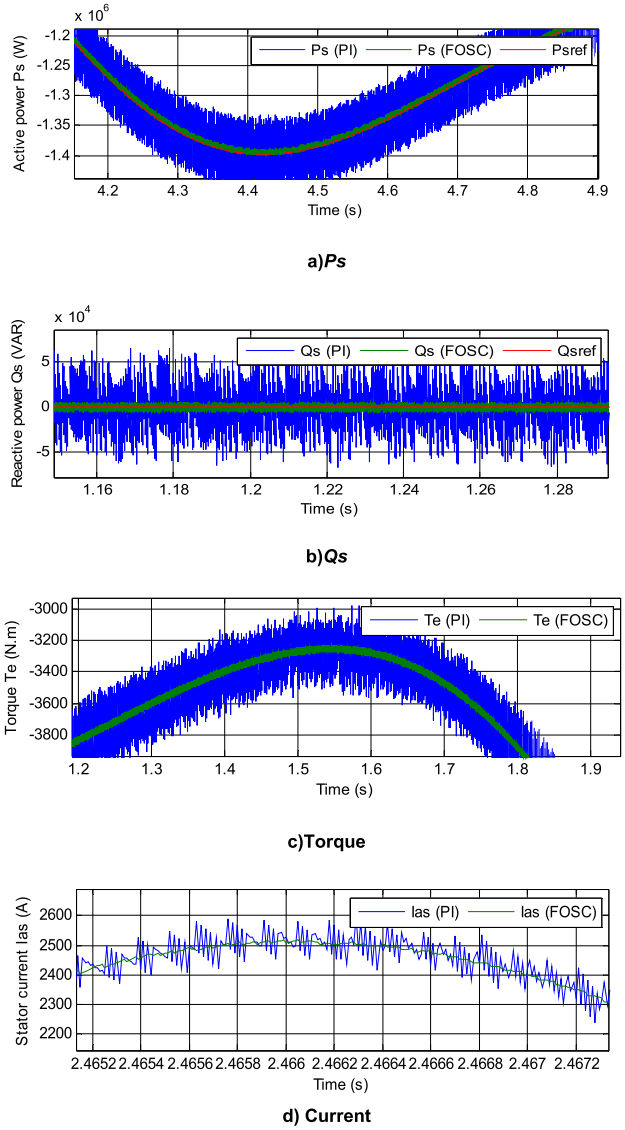

FIGURE 15. Zoom in the Qs, current, torque, and Ps (Third test).

the THD of the current compared to some techniques such as DPC, FOC, and DPC-PI. Accordingly, it can be said that the DPC-FOSC is among the best techniques to be proposed for controlling electrical machinesAdditionally, the use of the DPC-FOSC has been seen in the field of renewable energy, as well as in the enhancement of power quality.

In Tables 9 and 10, a comparison between DPC-FOSC and some existing controls used in wind energy is presented in terms of power ripple reduction ratios and response times for *Ps* and *Qs*. These two tables provide a clear picture of the distinguished performance and high efficiency that characterize the proposed strategy in reducing ripple values by very high percentages compared to those in some works. In addition, the response time provided is the best and shortest for *Ps* and *Qs* compared to the times

TABLE 8. Comparison of the obtained results with those reported in reference control schemes proposed in the literature.

References	Methods	THD (%)
[9]	DPC-HOSMC	1.66
[41]	DTC	2.57
	DTC-SOCSM	0.98
[42]	DPC	8.87
	DPC with neural algorithm	2.91
	DPC with neuro-fuzzy algorithm	2.72
[43]	DTC	6.70
	Fuzzy DTC	2.04
[44]	FSMC	3.1
[45]	Intelligent DTC	4.80
[46]	Predictive polar flux control	0.77
	Predictive DTC	2.15
[47]	DPC using L-filter	10.79
	DPC using LCL-filter	4.05
[48]	FOC with Type 2 FLC	1.14
[49]	ISMC	9.7
	Multi-resonant-based SMC	3.2
[50]	SOSMC	3.13
[51]	DTC-PI	12
	DTC with intelligent control	7.19
[52]	FOC	3.70
[53]	FOC-PI	1.39
	ISMC	0.88
[54]	Virtual flux DPC	4.88
	DPC	4.19
	Fist test	0.13
DPC-FOSC strategy	Second test	0.16
	Third test	0.20

TABLE 9. Comparison in terms of energy ripple reduction rates.

References and techniques		Ratios (%)	
		Ps ripples	*Qs* ripples
DPC-FOSC technique	First test	91.66%	93.19%
	Second test	99.17%	92%
	Third test	72.50%	93.72%
[57]	STA	21.75%	22.66%
	Modified STA	19.11%	21.23%
[48]	DPC-ANN	45.26%	66.29%
	DPC-NF	57.74%	67.13%
[55]	Intelligent control	36%	35%
[56]	Backstepping control	28.57%	46.93%
[23]		41.17%	94%

provided by some existing strategies. So these two tables refute everything mentioned above and make this strategy the appropriate solution in the future to control various industrial systems.

VI. CONCLUSION

In this study, a system for generating electric power from wind was proposed using MRWP, where an asynchronous

TABLE 10. Comparison in terms of response time reduction rates.

References		Time Response (ms)	
		Ps (W)	*Qs* (VAR)
[58]		33.8 ms	34.5 ms
[53]		-	28 ms
[59]		32 ms	-
[60]		15 ms	80 ms
[61]	DPC	17 ms	18 ms
	Nonlinear DPC	9 ms	5 ms
[55]	PI-NN	4.52 ms	26.26 ms
DPC-FOSC	First test	6.58 ms	6.57 ms
	Second test	4.386 ms	4.43 ms
	Third test	3.12 ms	3.09 ms

generator is used to generate electricity. This system is controlled by a new control characterized by durability, simplicity, and ease of implementation to raise the quality of power and current and improve the effectiveness of the system in the closed loop. To boost the performance indicators of the AG-MRWP system, the suggested control method combines DPC, synergetic control, and fractional-order control. This combination exploits the advantages of each strategy. The advantages of the DPC are its simplicity, quick dynamic reaction, and ease of implementation. The synergetic control, lesseneffectively attenuating power ripples, and lessening the chattering phenomena issue. To address the drawbacks of the DPC and enhance the quality of the current output, fractional calculus is advantageous.

Two different wind speed behaviors were chosen to study all AG operating modes and verify the robustness of the DPC-FOSC. Random WS behavior was chosen to cause AG to operate in several operating modes (sub, super, and simultaneous modes). In addition, a third test was proposed to study the robustness characteristics of the DPC-FOSC in case of system parameter changes, and the results and high performance of the DPC-FOSC were compared with the results of the DPC represented by DPC-PI. The simulation results showed the high performance of the DPC-FOSC in minimizing the active power and torque ripples, good dynamic responses, and low THD (<0.16%) of the generated current with a fixed network frequency of 50 Hz. Future publications will focus on applying artificial intelligence methods, such as neural networks, to suggest more effective ways that may be applied to other electrical machines.

APPENDIX

A. PARAMETERS OF THE PROPOSED CONTROLLER

Table 11 represents the FOSC parameters used to control the AG power, where the values used are the same as those used for the *Ps* and *Qs*.

TABLE 11. Parameters of the FOSC.

	Parameters	Values
Active power controller	μ	0.75
	T	100
Reactive power controller	μ	0.75
	T	100

B. PARAMETERS OF THE MRWP SYSTEM

Table 12 represents the parameters used in the numerical simulation of the MRWP system.

TABLE 12. Parameters of the MRWP system.

Parameters	Valeur
Numbers of turbine blades.	3
Number of secondary turbine blades	3
R_2	25.5 m
R_1	13.2 m
r_1	1 m
r_2	0.5 m
r_g	0.75 m
J_2	1000 Kg.m^2
J_1	500 Kg.m^2

REFERENCES

[1] B. Habib, "Direct active and reactive powers command with third-order sliding mode theory for DFIG-based dual-rotor wind power systems," *Int. J. Natural Eng. Sci.*, vol. 15, no. 1, pp. 17–34, 2021.
[2] R. M. Prasad and M. A. Mulla, "Rotor position-sensorless algorithms for direct power control of rotor-tied DFIG," *IEEE Trans. Power Electron.*, vol. 36, no. 6, pp. 6213–6217, Jun. 2021, doi: 10.1109/TPEL.2020.3040705.
[3] H. Nian, P. Cheng, and Z. Q. Zhu, "Coordinated direct power control of DFIG system without phase-locked loop under unbalanced grid voltage conditions," *IEEE Trans. Power Electron.*, vol. 31, no. 4, pp. 2905–2918, Apr. 2016, doi: 10.1109/tpel.2015.2453127.
[4] J. Hu, H. Nian, B. Hu, Y. He, and Z. Q. Zhu, "Direct active and reactive power regulation of DFIG using sliding-mode control approach," *IEEE Trans. Energy Convers.*, vol. 25, no. 4, pp. 1028–1039, Dec. 2010, doi: 10.1109/TEC.2010.2048754.
[5] P. Xiong and D. Sun, "Backstepping-based DPC strategy of a wind turbine-driven DFIG under normal and harmonic grid voltage," *IEEE Trans. Power Electron.*, vol. 31, no. 6, pp. 4216–4225, Jun. 2016, doi: 10.1109/TPEL.2015.2477442.
[6] J. Han, Z. Liu, and N. Liang, "Nonlinear adaptive robust control strategy of doubly fed induction generator based on virtual synchronous generator," *IEEE Access*, vol. 8, pp. 159887–159896, 2020, doi: 10.1109/ACCESS.2020.2994094.
[7] X. Wang, D. Sun, and Z. Q. Zhu, "Resonant-based backstepping direct power control strategy for DFIG under both balanced and unbalanced grid conditions," *IEEE Trans. Ind. Appl.*, vol. 53, no. 5, pp. 4821–4830, Sep. 2017, doi: 10.1109/TIA.2017.2700280.
[8] D. Sun, X. Wang, H. Nian, and Z. Q. Zhu, "A sliding-mode direct power control strategy for DFIG under both balanced and unbalanced grid conditions using extended active power," *IEEE Trans. Power Electron.*, vol. 33, no. 2, pp. 1313–1322, Feb. 2018, doi: 10.1109/TPEL.2017.2686980.
[9] I. Yaichi, A. Semmah, P. Wira, and Y. Djeriri, "Super-twisting sliding mode control of a doubly-fed induction generator based on the SVM strategy," *Periodica Polytechnica Electr. Eng. Comput. Sci.*, vol. 63, no. 3, pp. 178–190, Jun. 2019, doi: 10.3311/ppee.13726.
[10] H. Benbouhenni, "Synergetic control theory scheme for asynchronous generator based dual-rotor wind power," *J. Electr. Eng., Electron. Control Comput. Sci*, vol. 7, no. 3, pp. 19–28, 2021.

[11] H. Benbouhenni, Z. Boudjema, and A. Belaidi, "Direct power control with NSTSM algorithm for DFIG using SVPWM technique," *Iranian J. Electr. Electron. Eng.*, vol. 17, no. 1, pp. 1–11, 2021, doi: 10.22068/IJEEE.17.1.1518.

[12] H. Afghoul, D. Chikouche, F. Krim, B. Babes, and A. Beddar, "Implementation of fractional-order integral-plus-proportional controller to enhance the power quality of an electrical grid," *Electric Power Compon. Syst.*, vol. 44, no. 9, pp. 1018–1028, May 2016, doi: 10.1080/15325008.2016.1147509.

[13] R. Errouissi, A. Al-Durra, S. M. Muyeen, S. Leng, and F. Blaabjerg, "Offset-free direct power control of DFIG under continuous-time model predictive control," *IEEE Trans. Power Electron.*, vol. 32, no. 3, pp. 2265–2277, Mar. 2017, doi: 10.1109/TPEL.2016.2557964.

[14] S. Khateri-abri, S. Tohidi, and N. Rostami, "Improved direct power control of DFIG wind turbine by using a fuzzy logic controller," in *Proc. 10th Int. Power Electron., Drive Syst. Technol. Conf. (PEDSTC)*, Feb. 2019, pp. 458–463, doi: 10.1109/pedstc.2019.8697581.

[15] M. N. Uddin, Md. S. Arifin, and N. Rezaei, "A novel neuro-fuzzy based direct power control of a DFIG based wind farm incorporated with distance protection scheme and LVRT capability," in *Proc. IEEE Ind. Appl. Soc. Annu. Meeting (IAS)*, Detroit, MI, USA, Oct. 2022, pp. 1–8, doi: 10.1109/IAS54023.2022.9939684.

[16] J. Mohammadi, S. Vaez-Zadeh, S. Afsharnia, and E. Daryabeigi, "A combined vector and direct power control for DFIG-based wind turbines," *IEEE Trans. Sustain. Energy*, vol. 5, no. 3, pp. 767–775, Jul. 2014, doi: 10.1109/TSTE.2014.2301675.

[17] K. Xiahou, M. S. Li, Y. Liu, and Q. H. Wu, "Sensor fault tolerance enhancement of DFIG-WTs via perturbation observer-based DPC and two-stage Kalman filters," *IEEE Trans. Energy Convers.*, vol. 33, no. 2, pp. 483–495, Jun. 2018, doi: 10.1109/TEC.2017.2771250.

[18] X. Wang and D. Sun, "Three-vector-based low-complexity model predictive direct power control strategy for doubly fed induction generators," *IEEE Trans. Power Electron.*, vol. 32, no. 1, pp. 773–782, Jan. 2017, doi: 10.1109/TPEL.2016.2532387.

[19] L. Xiao, L. Zhang, F. Gao, and J. Qian, "Robust fault-tolerant synergetic control for dual three-phase PMSM drives considering speed sensor fault," *IEEE Access*, vol. 8, pp. 78912–78922, 2020, doi: 10.1109/ACCESS.2020.2989821.

[20] A. Elnady, A. Noureldin, and A. A. Adam, "Improved synergetic current control for grid-connected microgrids and distributed generation systems," *J. Modern Power Syst. Clean Energy*, vol. 10, no. 5, pp. 1302–1313, Sep. 2022, doi: 10.35833/MPCE.2021.000336.

[21] Y. S. Hagh, A. Fekih, and H. Handroos, "Robust PI-based non-singular terminal synergetic control for nonlinear systems via hybrid nonlinear disturbance observer," *IEEE Access*, vol. 9, pp. 97401–97414, 2021, doi: 10.1109/ACCESS.2021.3094554.

[22] H. Benbouhenni and N. Bizon, "Terminal synergetic control for direct active and reactive powers in asynchronous generator-based dual-rotor wind power systems," *Electronics*, vol. 10, no. 16, p. 1880, Aug. 2021, doi: 10.3390/electronics10161880.

[23] H. Benbouhenni, F. Mehedi, and L. Soufiane, "New direct power synergetic-SMC technique based PWM for DFIG integrated to a variable speed dual-rotor wind power," *Automatika*, vol. 63, no. 4, pp. 718–731, Dec. 2022, doi: 10.1080/00051144.2022.2065801.

[24] H. Benbouhenni and N. Bizon, "A synergetic sliding mode controller applied to direct field-oriented control of induction generator-based variable speed dual-rotor wind turbines," *Energies*, vol. 14, no. 15, p. 4437, Jul. 2021, doi: 10.3390/en14154437.

[25] H. Benbouhenni and S. Lemdani, "Combining synergetic control and super twisting algorithm to reduce the active power undulations of doubly fed induction generator for dual-rotor wind turbine system," *Electr. Eng. Electromechanics*, vol. 2021, no. 3, pp. 8–17, Jun. 2021, doi: 10.20998/2074-272x.2021.3.02.

[26] H. Benbouhenni and H. Gasmi, "Comparative study of synergetic controller with super twisting algorithm for rotor side inverter of DFIG," *Int. J. Smart Grid*, vol. 6, no. 4, pp. 144–156, 2022, doi: 10.20508/ijsmartgrid.v6i4.265.g251.

[27] Z. Xie, X. Gao, S. Yang, and X. Zhang, "Improved fractional-order damping method for voltage-controlled DFIG system under weak grid," *J. Modern Power Syst. Clean Energy*, vol. 10, no. 6, pp. 1531–1541, Nov. 2022, doi: 10.35833/MPCE.2020.000843.

[28] K. Xiahou, Y. Liu, L. Wang, M. S. Li, and Q. H. Wu, "Control of DFIG's rotor-side converter with decoupling of current loops using observer-based fractional-order sliding-mode regulators," *IEEE Access*, vol. 7, pp. 163412–163420, 2019, doi: 10.1109/ACCESS.2019.2952589.

[29] R. Li, F. Wu, P. Hou, and H. Zou, "Performance assessment of FO-PID temperature control system using a fractional order LQG benchmark," *IEEE Access*, vol. 8, pp. 116653–116662, 2020, doi: 10.1109/ACCESS.2020.3004701.

[30] M. I. Mosaad, A. Abu-Siada, and M. F. El-Naggar, "Application of superconductors to improve the performance of DFIG-based WECS," *IEEE Access*, vol. 7, pp. 103760–103769, 2019, doi: 10.1109/ACCESS.2019.2929261.

[31] M. V. Kazemi, S. J. Sadati, and S. A. Gholamian, "Adaptive frequency control of microgrid based on fractional order control and a data-driven control with stability analysis," *IEEE Trans. Smart Grid*, vol. 13, no. 1, pp. 381–392, Jan. 2022, doi: 10.1109/TSG.2021.3109627.

[32] H. Dong, M. Su, K. Liu, and W. Zou, "Mitigation strategy of subsynchronous oscillation based on fractional-order sliding mode control for VSC-MTDC systems with DFIG-based wind farm access," *IEEE Access*, vol. 8, pp. 209242–209250, 2020, doi: 10.1109/ACCESS.2020.3038665.

[33] L. Xiong, J. Wang, X. Mi, and M. W. Khan, "Fractional order sliding mode based direct power control of grid-connected DFIG," *IEEE Trans. Power Syst.*, vol. 33, no. 3, pp. 3087–3096, May 2018, doi: 10.1109/TPWRS.2017.2761815.

[34] N. Ullah, M. Asghar Ali, A. Ibeas, and J. Herrera, "Adaptive fractional order terminal sliding mode control of a doubly fed induction generator-based wind energy system," *IEEE Access*, vol. 5, pp. 21368–21381, 2017, doi: 10.1109/ACCESS.2017.2759579.

[35] N. Ullah, I. Sami, Md. S. Chowdhury, K. Techato, and H. I. Alkhammash, "Artificial intelligence integrated fractional order control of doubly fed induction generator-based wind energy system," *IEEE Access*, vol. 9, pp. 5734–5748, 2021, doi: 10.1109/ACCESS.2020.3048420.

[36] H. Benbouhenni, N. Bizon, I. Colak, P. Thounthong, and N. Takorabet, "Application of fractional-order PI controllers and neuro-fuzzy PWM technique to multi-rotor wind turbine systems," *Electronics*, vol. 11, no. 9, p. 1340, Apr. 2022, doi: 10.3390/electronics11091340.

[37] H. Gasmi, S. Mendaci, S. Laifa, W. Kantas, and H. Benbouhenni, "Fractional-order proportional-integral super twisting sliding mode controller for wind energy conversion system equipped with doubly fed induction generator," *J. Power Electron.*, vol. 22, no. 8, pp. 1357–1373, Aug. 2022, doi: 10.1007/s43236-022-00430-0.

[38] A. D. Falehi, "Optimal power tracking of DFIG-based wind turbine using MOGWO-based fractional-order sliding mode controller," *ASME. J. Sol. Energy Eng.*, vol. 142, no. 3, Jun. 2020, Art. no. 031004, doi: 10.1115/1.4044977.

[39] A. D. Falehi and M. Rafiee, "LVRT/HVRT capability enhancement of DFIG wind turbine using optimal design and control of novel PID-AMLI based DVR," *Sustain. Energy, Grids Netw.*, vol. 16, pp. 111–125, Dec. 2018, doi: 10.1016/j.segan.2018.06.001.

[40] A. D. Falehi and H. Torkaman, "Promoted supercapacitor control scheme based on robust fractional-order super-twisting sliding mode control for dynamic voltage restorer to enhance FRT and PQ capabilities of DFIG-based wind turbine," *J. Energy Storage*, vol. 42, Oct. 2021, Art. no. 102983, doi: 10.1016/j.est.2021.102983.

[41] Z. Boudjema, R. Taleb, Y. Djeriri, and A. Yahdou, "A novel direct torque control using second order continuous sliding mode of a doubly fed induction generator for a wind energy conversion system," *Turkish J. Electr. Eng. Comput. Sci.*, vol. 25, pp. 965–975, 2017, doi: 10.3906/elk-1510-89.

[42] Y. Sahri, S. Tamalouzt, F. Hamoudi, S. L. Belaid, M. Bajaj, M. M. Alharthi, M. S. Alzaidi, and S. S. M. Ghoneim, "New intelligent direct power control of DFIG-based wind conversion system by using machine learning under variations of all operating and compensation modes," *Energy Rep.*, vol. 7, pp. 6394–6412, Nov. 2021, doi: 10.1016/j.egyr.2021.09.075.

[43] W. Ayrir, M. Ourahou, B. El Hassouni, and A. Haddi, "Direct torque control improvement of a variable speed DFIG based on a fuzzy inference system," *Math. Comput. Simul.*, vol. 167, pp. 308–324, Jan. 2020, doi: 10.1016/j.matcom.2018.05.014.

[44] Z. Boudjema, A. Meroufel, Y. Djerriri, and E. Bounadja, "Fuzzy sliding mode control of a doubly fed induction generator for wind energy conversion," *Carpathian J. Electron. Comput. Eng.*, vol. 6, no. 2, pp. 7–14, 2013, doi: 10.11591/ijpeds.v10.i3.pp1592-1602.

[45] S. Mahfoud, A. Derouich, N. E. Ouanjli, M. E. Mahfoud, and M. Taoussi, "A new strategy-based PID controller optimized by genetic algorithm for DTC of the doubly fed induction motor," *Systems*, vol. 9, no. 2, p. 37, May 2021, doi: 10.3390/systems9020037.
[46] M. A. Mossa, H. Echeikh, and A. Iqbal, "Enhanced control technique for a sensor-less wind driven doubly fed induction generator for energy conversion purpose," *Energy Rep.*, vol. 7, pp. 5815–5833, Nov. 2021, doi: 10.1016/j.egyr.2021.08.183.
[47] M. M. Alhato and S. Bouallègue, "Direct power control optimization for doubly fed induction generator based wind turbine systems," *Math. Comput. Appl.*, vol. 24, no. 3, p. 77, Aug. 2019, doi: 10.3390/mca24030077.
[48] F. Amrane and A. Chaiba, "A novel direct power control for grid-connected doubly fed induction generator based on hybrid artificial intelligent control with space vector modulation," *Rev. Roum. Sci. Techn.-Electrotechn. Et Energ*, vol. 61, no. 3, pp. 263–268, 2016.
[49] Y. Quan, L. Hang, Y. He, and Y. Zhang, "Multi-resonant-based sliding mode control of DFIG-based wind system under unbalanced and harmonic network conditions," *Appl. Sci.*, vol. 9, no. 6, p. 1124, Mar. 2019, doi: 10.3390/app9061124.
[50] A. Yahdou, B. Hemici, and Z. Boudjema, "Second order sliding mode control of a dual-rotor wind turbine system by employing a matrix converter," *J. Electr. Eng.*, vol. 16, pp. 1–11, Jan. 2016.
[51] S. Mahfoud, A. Derouich, A. Iqbal, and N. El Ouanjli, "ANT-colony optimization-direct torque control for a doubly fed induction motor: An experimental validation," *Energy Rep.*, vol. 8, pp. 81–98, Nov. 2022, doi: 10.1016/j.egyr.2021.11.239.
[52] F. Amrane, A. Chaiba, B. Babes, and S. Mekhilef, "Design and implementation of high performance field oriented control for grid-connected doubly fed induction generator via hysteresis rotor current controller," *Rev. Roum. Sci. Techn.-Electrotechn. Et Energ*, vol. 61, no. 4, pp. 319–324, 2016.
[53] H. Chojaa, A. Derouich, S. E. Chehaidia, O. Zamzoum, M. Taoussi, and H. Elouatouat, "Integral sliding mode control for DFIG based WECS with MPPT based on artificial neural network under a real wind profile," *Energy Rep.*, vol. 7, pp. 4809–4824, Nov. 2021, doi: 10.1016/j.egyr.2021.07.066.
[54] N. A. Yusoff, A. M. Razali, K. A. Karim, T. Sutikno, and A. Jidin, "A concept of virtual-flux direct power control of three-phase AC-DC converter," *Int. J. Power Electron. Drive Syst.*, vol. 8, no. 4, pp. 1776–1784, 2017, doi: 10.11591/ijpeds.v8.i4.pp1776-1784.
[55] H. Benbouhenni, H. Gasmi, and I. Colak, "Intelligent control scheme of asynchronous generator-based dual-rotor wind power system under different working conditions," *Majlesi J. Energy Manag.*, vol. 11, no. 3, pp. 8–15, 2022. [Online]. Available: https://em.majlesi.info/index.php/em/article/view/494
[56] H. Benbouhenni, H. Gasmi, and I. Colak, "Backstepping control for multi-rotor wind power systems," *Majlesi J. Energy Manage.*, vol. 11, no. 4, pp. 8–15, 2022. [Online]. Available: https://em.majlesi.info/index.php/em/article/view/493
[57] R. Hiremath and T. Moger, "Modified super twisting algorithm based sliding mode control for LVRT enhancement of DFIG driven wind system," *Energy Rep.*, vol. 8, pp. 3600–3613, Nov. 2022, doi: 10.1016/j.egyr.2022.02.235.
[58] F. Echiheb, Y. Ihedrane, B. Bossoufi, M. Bouderbala, S. Motahhir, M. Masud, S. Aljahdali, and M. ElGhamrasni, "Robust sliding-backstepping mode control of a wind system based on the DFIG generator," *Sci. Rep.*, vol. 12, no. 1, p. 11782, Jul. 2022, doi: 10.1038/s41598-022-15960-7.
[59] B. Bossoufi, M. Karim, A. Lagrioui, and M. Taoussi, "FPGA-based implementation nonlinear backstepping control of a PMSM drive," *IJPEDS Int. J. Power Electron. Drive Syst.*, vol. 4, no. 1, pp. 12–23, 2014.
[60] H. E. Alami, B. Bossoufi, S. Motahhir, E. H. Alkhammash, M. Masud, M. Karim, M. Taoussi, M. Bouderbala, M. Lamnadi, and M. El Mahfoud, "FPGA in the loop implementation for observer sliding mode control of dfig-generators for wind turbines," *Electronics*, vol. 11, p. 116, Nov. 2022, doi: 10.3390/electronics11010116.
[61] Y. Ibrahim, A. Semmah, and W. Patrice, "Neuro-second order sliding mode control of a dfig based wind turbine system," *J. Electr. Electron. Eng.*, vol. 13, no. 1, pp. 63–68, 2020.